April 2002 • NREL/SR-520-32072

Subcontractor Report

Photovoltaic Manufacturing Cost and Throughput Improvements for Thin Film CIGS-Based Modules

Final Technical Report
July 1998 – September 2001

J. Britt
Global Solar Energy
Tucson, Arizona

National Renewable Energy Laboratory

1617 Cole Boulevard
Golden, Colorado 80401-3393

NREL is a U.S. Department of Energy Laboratory
Operated by Midwest Research Institute • Battelle • Bechtel

Contract No. DE-AC36-99-GO10337

April 2002 • NREL/SR-520-32072

Photovoltaic Manufacturing Cost and Throughput Improvements for Thin Film CIGS-Based Modules

Final Technical Report
July 1998 – September 2001

J. Britt
Global Solar Energy
Tucson, Arizona

NREL Technical Monitor: R.L. Mitchell

Prepared under Subcontract No. ZAX-8-17647-11

National Renewable Energy Laboratory

1617 Cole Boulevard
Golden, Colorado 80401-3393

NREL is a U.S. Department of Energy Laboratory
Operated by Midwest Research Institute • Battelle • Bechtel

Contract No. DE-AC36-99-GO10337

NOTICE

This report was prepared as an account of work sponsored by an agency of the United States government. Neither the United States government nor any agency thereof, nor any of their employees, makes any warranty, express or implied, or assumes any legal liability or responsibility for the accuracy, completeness, or usefulness of any information, apparatus, product, or process disclosed, or represents that its use would not infringe privately owned rights. Reference herein to any specific commercial product, process, or service by trade name, trademark, manufacturer, or otherwise does not necessarily constitute or imply its endorsement, recommendation, or favoring by the United States government or any agency thereof. The views and opinions of authors expressed herein do not necessarily state or reflect those of the United States government or any agency thereof.

Available electronically at http://www.osti.gov/bridge

Available for a processing fee to U.S. Department of Energy
and its contractors, in paper, from:
U.S. Department of Energy
Office of Scientific and Technical Information
P.O. Box 62
Oak Ridge, TN 37831-0062
phone: 865.576.8401
fax: 865.576.5728
email: reports@adonis.osti.gov

Available for sale to the public, in paper, from:
U.S. Department of Commerce
National Technical Information Service
5285 Port Royal Road
Springfield, VA 22161
phone: 800.553.6847
fax: 703.605.6900
email: orders@ntis.fedworld.gov
online ordering: http://www.ntis.gov/ordering.htm

Printed on paper containing at least 50% wastepaper, including 20% postconsumer waste

Table of Contents

List of Figures iv
List of Tables vii
References viii
1.0 Inkjet/Laser Process Integration and Optimization 1
1.1 Introduction 1
1.2 Objectives 2
1.3 Technical Approach 3
1.4 Accomplishments 3
High-speed All-laser Scribing Processes 3
Inkjet Technology for Insulator Deposition 4
Improvements in Reliability and Robustness 4
Increased Throughput 7
Scribe Compression—Minimizing Total Area Loss 8
1.5 Summary 9
1.6 Alternate Back Contact (Addendum) 10
2.0 Incorporation of High-rate CIGS Deposition 12
2.1 Introduction 12
2.2 Objectives 12
2.3 Technical Approach 13
2.4 Accomplishments 14
Effusion Source 14
High-rate CIGS Deposition 17
Se Consumption and Delivery 18
2.5 Summary 24
3.0 Realtime, Intelligent Control of CIGS Deposition 25
3.1 Parallel Detector Spectroscopic Ellipsometer (PDSE) 25
Introduction 25
Objectives 25
Technical Approach 26
Accomplishments 26
PDSE Hardware Development 27

PDSE IR Capability 31
PDSE Alignment and Calibration 33
PDSE Hardware Installation in CIGS Production Deposition Chamber 35
PDSE Algorithm and Process Control Demonstrations 36
Summary 37
3.2 X-ray Fluorescometry (XRF) 37
Background 37
Hardware Installation 38
Control Strategy 38
Accomplishments 38
Summary 40
4.0 Conclusions 41

List of Figures

Figure 1.1 The post-absorber monolithic interconnect structure used at GSE 1

Figure 1.2 A comparison of measured output module voltage vs. module voltage expected from small area diodes results on the same web 5

Figure 1.3 Fill factor for small area devices isolated by laser scribing the front TCO contact at various beam power density settings 6

Figure 1.4 Indicated Jsc of small area devices isolated by laser scribing the front TCO contact at various beam power density settings 6

Figure 1.5 Optical micrograph showing the start (a) middle (b) and end (c) of an inkjet deposited line made using smaller dispense tip orifices. The linewidth in the region shown in the center image is 100 microns. 7

Figure 1.6 An SEM micrograph of a monolithic interconnect made on polyimide based CIGS using the GSE all-laser scribing and inkjet processes..... 8

Figure 1.7 A flexible, lightweight monolithically integrated CIGS module on polyimide in a 12-inch x 32-inch format having more than 300 volts output under outdoor illumination conditions..... 9

Figure 1.8 An SEM micrograph of cracks formed in the Mo back contact (CIGS absorber layer has been pulled off) 10

Figure 1.9 A higher magnification image of the cracks shown in Fig 1.8 above..... 11

Figure 2.1 Cu/(Ga+In) by EDS (20kV) for five consecutive lots (center only)..... 15

Figure 2.2 Ga/(Ga+In) by EDS (20kV) for five consecutive lots (center only)..... 16

Figure 2.3 CIGS thickness by SEM x-section for five consecutive lots (center only)..... 16

Figure 2.4 Cu/(Ga+In) uniformity at web speeds of 6, 8, and 10 inches/min. 18

Figure 2.5 Ga/(Ga+In) uniformity at web speeds of 6, 8, and 10 inches/min. 18

Figure 2.6 In thickness and Se pot power as a function of run time for heater configuration 1 19

Figure 2.7 In thickness and Se pot power as a function of run time for heater configuration 2 19

Figure 2.8 In thickness and Se pot power as a function of run time for heater configuration 3 20

Figure 2.9 Se pot power and In thickness as a function of elapsed run time..... 20

Figure 2.10 Se sensor output and Se pot power as a function of elapsed run time 21

Figure 2.11 Histogram of Se control response (506SA)..... 22

Figure 2.12 In thickness and Se sensor output as a function of run time (517SA) 22

Figure 2.13 Se control response demonstrated during a DOE run 23

Figure 2.14 Se consumption rate before and after the delivery system redesign 24

Figure 3.1 Angular (a) and intensity (b) comparison of a standard 1 mm diameter optical fiber and 1 mm to 2 mm diameter fiber taper..... 29

Figure 3.2 Measured angular dependence of an 80 degree elliptical, 10 degree elliptical and standard cosine diffuser with a 1 mm diameter optical fiber (a) and a 2 mm fiber taper (b) 30

Figure 3.3 Angular sensitivity of 80 degree elliptical diffuser with 2 mm fiber taper and standard diffuser/ optical fiber over a 40 degree span (a), and normalized throughput intensity comparison between 80 degree elliptical diffuser with fiber taper and standard diffuser/ optical fiber arrangement (b) 30

Figure 3.4 Measured angular dependence of PDSE data from Si with 80 degree elliptical (a), 10 degree elliptical (b) and no diffuser (c). The data indicate that the PDSE has the least alignment sensitivity with the 80 degree diffusers and the greatest with no diffusers. Furthermore, the data indicate that the 10 degree diffusers provide a good compromise between the two by substantially increasing signal to noise while decreasing alignment sensitivity. 31

Figure 3.5 Spectra simultaneously collected by two IR spectrometers 31

Figure 3.6 An optical fiber switch was designed and constructed to collect four PDSE polarization states with one spectrometer (a), and comparison of data collected from Si with a standard SE and the PDSE using an optical switch and one spectrometer (b) 32

Figure 3.7 Simultaneously measured IR spectra from four PDSE channels. This represents the first time that complete polarization state information was collected using four IR spectrometers simultaneously..... 33

Figure 3.8 Measured CIGS ellipsometry data using the PDSE with four IR spectrometers to simultaneously collect four polarization states. The data were collected in real-time as the CIGS sample moved past the PDSE detection system. The slight shift in the data along with slightly different shapes indicates that the PDSE is very sensitive to film thickness (possibly on the order of a few angstroms resolution) and other optical and electronic film properties that are present even in a very good CIGS sample..... 33

Figure 3.9 In-situ real-time PDSE data acquired from a moving flexible stainless steel substrate. While the PDSE accurately corrected for vibration, defective wrinkles in the substrate caused misalignment that could not be corrected for with the present alignment system. The data indicate that once the wrinkle passes the PDSE, the original alignment is regained and the measurement is again accurate. 36

Figure 3.10 Film thickness (a) and band gap (b) calculated with real-time processing interpretive algorithms from data measured as a CIGS thin film is moved passed the PDSE..... 37

Figure 3.11 Elemental thicknesses of Cu, Ga, and In measured by XRF during a 315-foot deposition conducted under XRF feedback control 39
Figure 3.12 Composition ratios for the same deposition 39
Figure 3.13 Temperature set point changes for Ga and In sources under XRF control 40
Figure 3.14 Temperature set point changes for the Cu source under XRF control 40

List of Tables

Table 1.1 Alternate back contact compared to a Mo back contact..... 11
Table 2.1 Cu and In delivery efficiency across multiple lots at program end..... 17
Table 2.2 Metals consumption rates at program end..... 17
Table 2.3 Steady-state power consumption of effusion sources at program end..... 17
Table 2.4 Selenium utilization and average diode efficiency for two consecutive lots..... 23

References

[2-1] Private Communication, M. Contreras

[2-2] M. Bodegard and L. Stolt, Proceedings of the 12th EC Photovoltaic Solar Energy Conference (1994) 1743.

[2-3] V. Probst, J. Rimmasch, W. Stetter, H. Harms, W. Riedl, J. Holz and F. Karg, Proceedings of the 13th EC Photovoltaic Solar Energy Conference (1995) 2123.

1.0 Inkjet/Laser Process Integration and Optimization

1.1 Introduction

For monolithic integration of CIGS-based modules on flexible polyimide substrates, GSE has developed an all-laser, inkjet process in which all steps take place after absorber (CIGS) deposition. Complexity in the post-absorber scribing approach is greater than a simple sequential cascade scribing method conventionally used because the post-absorber method requires an inkjet backfill operation over one scribe. However, the post-absorber method avoids formation of shunt-causing pinholes in the absorber layer due to scribing debris created by a back contact scribe prior to the CIGS deposition. The structure of the monolithic interconnect used at GSE is shown in Figure 1.1 below. Sequentially, the S1 (back contact) scribe, S2 (via or interconnect) scribe and the P1 (inkjet print over the back contact scribe) are accomplished after CIGS and CdS deposition. The partially processed material then receives the TCO front contact deposition before laser processing to cut the S3 (front contact scribe).

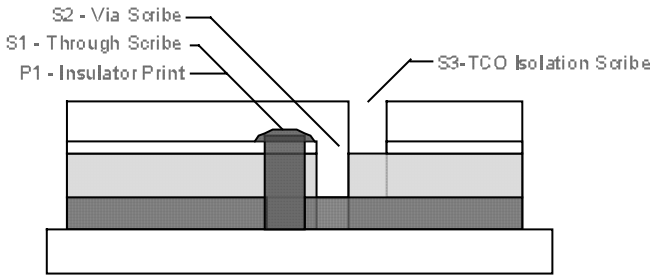

Figure 1.1 The post-absorber monolithic interconnect structure used at GSE

Although the via scribe need not be continuous, scribes for the back and front contact scribes must be continuous and well-controlled. The front contact scribe, in particular, must be selective, removing the front contact material cleanly without damage or shunt formation to the back contact. All-laser processing provides manufacturing advantages of increased speed, increased throughput, and reduced maintenance over mechanical scribing. Moreover, laser processing is virtually required for the selective cutting required in the post-absorber method on flexible polymer substrates. Mechanical scribing on compliant substrates invariably leads to shorting between the front and back contacts.

The post-absorber laser scribing approach requires that an insulating material be deposited over the back contact scribe, preventing direct shunt formation upon subsequent deposition of the TCO front contact. Screen printing is the technique conventionally used to deposit insulating material in the scribe, but it suffers from several drawbacks. Silk screen printing typically produces 250 to 1000 µm linewidths, which cause significant module area loss. Additionally, the screens stretch with use, causing registration errors and further loss in module area and manufacturing yield. Silk screen printing is also inflexible in that even small pattern changes require fabrication of completely new screens.

Inkjet technology was proposed as a method for controllably printing scribe areas with insulating lines while circumventing the limitations of screen printing. Conceptually, a single head or multiple heads capable of controllably dispensing a fine line of insulating material could be positioned and moved rapidly over a back contact scribe to generate a printed fill pattern.

Several types of inkjet technologies exist, including "bubble-jet," electrostatic/ultrasonic ink drop, and valved fluid dispense through an orifice. Each method is constrained by different limitations, such as speed, ultimate linewidth, and required fluid characteristics. For instance, the electrostatic/ultrasonic ink drop delivery is capable of very high printing speeds, but is very limited in the types of fluid it can dispense, having strict requirements for viscosity, surface tension, electrical conductivity and vapor pressure. Drying or curing time is also an important parameter for the printed insulator materials, because rapid processes for module production are needed for high throughput.

Success in this task depends on developing the equipment and process for rapidly depositing and drying insulating ink that is compatible with subsequent processes.

1.2 Objectives

Laser scribing is a major part of the patterning and integration process that enables module fabrication from large-area, thin-film CIGS PV material. Key issues with laser scribing are:

- Selective scribing of thin-film layers using all-laser methods
- Avoiding shunt formation due to scribe debris or edge effects in a heat affected zone
- Scribe speed and multiple beam delivery that affect throughput
- Scribe process tolerance and robustness

Key goals of this task are to:

- Develop robust, selective processes for front contact, back contact and interconnect scribes to improve yield
- Develop the equipment and methods to increase scribing speed to 23 cm/sec to improve throughput and cost
- Minimize scribe debris, scribe width and heat affected zone adjacent to scribe

Key issues for insulator deposition are:

- Linewidth and accuracy of the inkjet-deposited material
- Line continuity and uniformity of the inkjet-deposited material
- Overall process speed, including deposition rate and post-deposition curing time
- Insulating material compatibility with subsequent processes
- Insulating material properties of outgassing, adhesion, shrinkage, and resistivity

Key goals of the inkjet printing method are to:

- Assure reproducible, continuous, well-adherent lines of insulating material with uniform linewidths
- Obtain progressively decreasing ink-line-widths, to 125 microns, while maintaining line continuity and uniformity, and attain total interconnect widths (including all laser scribes) of 250 microns

- Develop the equipment and methods to minimize curing time and enable deposition rates of 22 cm/sec.
- Assure compatibility and integrate with all other module fabrication processes

1.3 Technical Approach

Commercial inkjet components have been adapted by GSE to deposit an insulating material in a fine, continuous line from a moving inkjet dispense head. The inkjet-deposited insulating material is applied during the first laser patterning operation (back contact and via scribe) directly in the previously cut back contact scribes, thus preventing formation of a direct short by the subsequent front contact deposition.

The largest challenge for Phase 2 was to improve equipment reliability and process robustness, as the existing equipment was prone to damage, clogging and drift in alignment after only brief periods of operation. The dispense tip or associated parts would typically clog before deposition of 100 to 200 lines. Additionally the line continuity was impacted strongly by small changes in operating parameters.

Additional challenges extending into Phase 3 were to improve total throughput, diminish inkjet linewidth and total interconnect width to meet PVMaT and corporate goals, and continue to demonstrate overall viability of monolithic integration in the face of changing conditions elsewhere in the process, such as CIGS thickness and properties or changes in the back contact. For instance, changes in the nature of the back contact necessitated re-optimization of the via scribing process. Evaluations of alternate inkjet subcomponents continued in Phase 3 to improve control, robustness and reliability. Alternate components were sourced from a diverse set of suppliers, ranging from component manufacturers for aerospace, to medical to semiconductor industries. Significantly improved throughput in the monolithic integration was achieved according to planned enhancements by using all four laser beams for scribing in both the first and second laser operations. Subsequently we incorporated dual inkjet heads, thus matching the intrinsic capability of four laser beams making four simultaneous scribes, of which two required subsequent inkjet coverage. Significant gains were incrementally achieved first by proving bidirectional scribing and inkjet capability, and then by merging hardware and software control to achieve inkjet coverage of the back contact scribe concurrent with the laser scribing, all in one integrated first laser operation, rather than in sequential laser and then inkjet operations.

Improvements in linewidth were addressed primarily by changing the inkjet dispense head to allow finer and better-controlled ink linewidths, and by improving the position-correction and fiducial-orientation software to more precisely align the entire module pattern prior to the second and final laser operation.

1.4 Accomplishments

High-speed All-laser Scribing Processes

During Phase 1, GSE successfully developed equipment and preliminary conditions that appeared to produce viable, all-laser, high speed (12-in/sec, 30.5-cm/sec) processes for the back contact, front contact and interconnect scribes for CIGS-based modules on flexible polyimide substrates. High-rate, selective, thin film cutting had been evidenced for these processes, and all

scribe processes were validated microstructurally by optical and scanning electron microscopic (SEM) examination. The high-rate back contact scribing process was partially validated through electrical tests. High-rate back contact scribes on flexible substrate under some process conditions were validated. Front contact and interconnect scribes underwent some electrical testing in addition to microstructural analysis. Microstructural analysis indicated that clean, selective removal of the TCO during the front contact scribe could be achieved under some process conditions. Results indicated the need for further optimization.

Remarkable process robustness was demonstrated during Phase 2 for both the back contact and front contact scribing processes. All laser scribes (P1, P2 and P3) were validated on a production laser scribing system through electrical tests for proper function. Improved capability was added to the scribing equipment, and the level of automation was increased. There remained a need for characterization of the scribing processes in even greater lot sizes, software and hardware augmentation to improve throughput, and study of the process window for the via (P2) process and front contact scribe over a greater range of laser powers and evaluation for tolerance to variation in absorber layer thickness.

Inkjet Technology for Insulator Deposition

In Phase 1, feasibility was demonstrated for GSE's inkjet technology, as evidenced by moderate numbers of deposited, continuous ink lines. The lines were deposited, (including drying time) at 30 cm/sec, which exceeded the PVMaT goal, with a linewidth that ranged typically from 200 to 400 µm.

Process robustness and equipment reliability were partially addressed in Phase 2. Although inkjet deposition of the insulating line was developed to handle rates of 30 cm/sec with high accuracy, further improvement was needed, including greater robustness, reliability and higher throughput of the inkjet operation to better match the rate associated with the laser operations. Plans were developed and partially implemented to provide for multiple inkjet heads, similar to the multiple laser beams for scribing. Software enhancements, including alterations for bidirectional inkjet capability were also planned, along with improvements aimed at equalizing the operating settings for multiple inkjet heads, and further reduction in deposited ink linewidth and decreased scribe spacing.

Improvements in Reliability and Robustness

Reliability has been improved by instituting uniform procedures for set-up, warm-up and adjustment of the laser head and beam delivery optics. Intervals have been established for monitoring and maintaining key parameters within specified limits. Even with these precautions, however, unacceptable or degraded scribe quality can occur. Fortunately, such instances are rare. The most extended instance of degraded scribe quality was traced to instability in beam quality and modal content. The problem was insidious in that it was intermittent and subtle, without obvious outward indications. We are better able to guard against such occurrences after having become familiar with their symptoms. Additionally, routine comparisons are done in the normal course of loss analysis for modules to compare those characteristics with the behavior projected from pads of small area diodes immediately adjacent to each module. An example in which some modules were sampled and compared with their expected output voltage to confirm proper operation of one scribing operation is shown in Figure 1.2 below. That figure compares

the measured open circuit module voltages to the expected module voltages. The expected module voltage was calculated as the product of the number of module segments and the average device Voc taken from device pads on either end of the module on the web. Modules for which adjacent device pads were not fabricated are labeled "OP_". The realization of module voltages comparable to those expected from device results served as another indication that scribe quality had been restored to within acceptable limits.

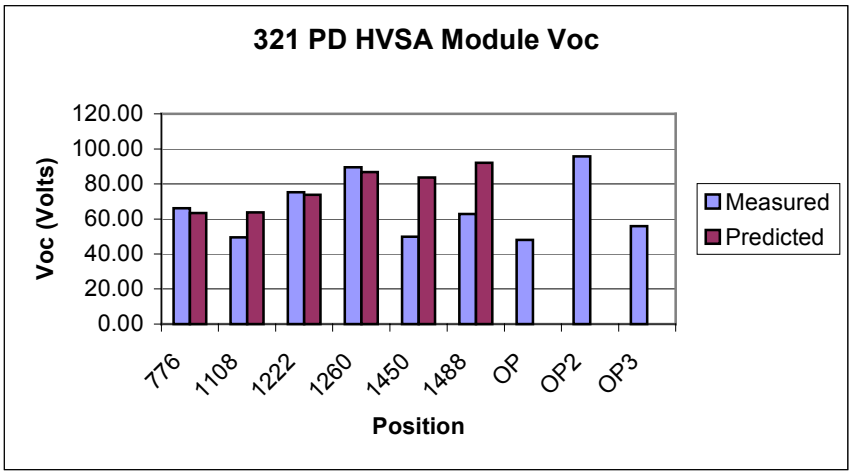

Figure 1.2 A comparison of measured output module voltage vs. module voltage expected from small area diodes results on the same web

Of course, a spare laser head is also maintained ready for operation in case of catastrophic failure or a problem that cannot be identified.

Several sources of unreliability were determined to arise from scribe misalignment of the second (front contact scribe) relative to the previously scribed back contact and via pattern. Simple registration of the two patterns using standard fiducial marks had gone well, and the patterns matched well at the datum points where both patterns originate. The patterns diverged progressively as scribing continued, and were only evident on the larger module designs (32-inch length). The effect appears to have resulted from a small stretching (about 600 parts/million) of the polyimide substrate under the tension used on the scribing station. The problem was probably not detected earlier because it only becomes of concern for very long, continuous module patterns such as those required for high voltage modules.

A dynamic scaling algorithm to eliminate scribe registration error due to web stretch or distortion between the first and second laser operations was implemented. The algorithm is executed by the motion system under software control based on a change in the position of additional fiducials on every module. The method actually expands or contracts the physical length of the second scribe pattern to match the existing first laser operation. The method has worked well, and scribe placement errors between first and second laser operations were less than 100 microns over a 32" long module using 260 module segments.

One other scribe registration error was traced to slight non-orthogonality of the scribed patterns, due to differential stretching from edge-to-edge in the 13-inch wide polyimide web. This error was essentially eliminated by a simple change in the placement of the pattern matching fiducials.

The front contact scribe process was re-evaluated for robustness over a significant range of operating conditions. CIGS material of uniform composition and reasonable quality was

selected for front contact scribes made over a wide range of laser power. Laser power is typically a critical parameter for front contact scribes. Power levels above or below an appropriate range either cause shunting back contact damage or incomplete device isolation. Anomalous or erratic behavior of device parameters such as fill factor and Jsc indicate the presence either shunting or leakage of current from adjacent cells. As shown in Figure 1.3 and Figure 1.4 below, the process window with the equipment in use at GSE is very broad: Beam power densities ranging from less than 70% up to 140% of the process setting produce acceptable front contact scribes.

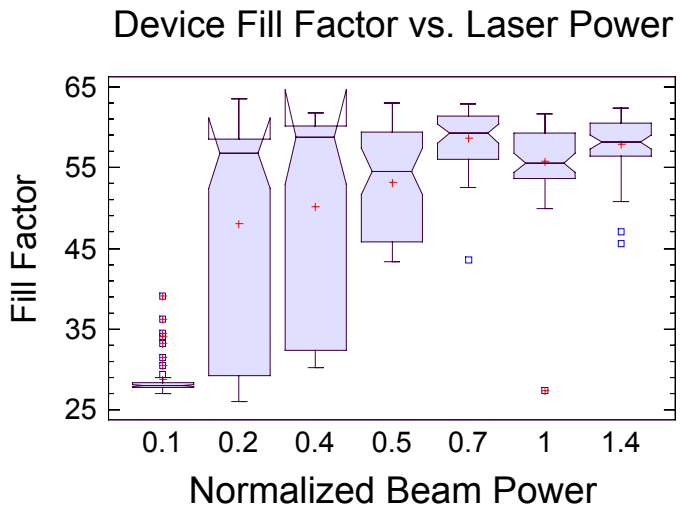

Figure 1.3 Fill factor for small area devices isolated by laser scribing the front TCO contact at various beam power density settings

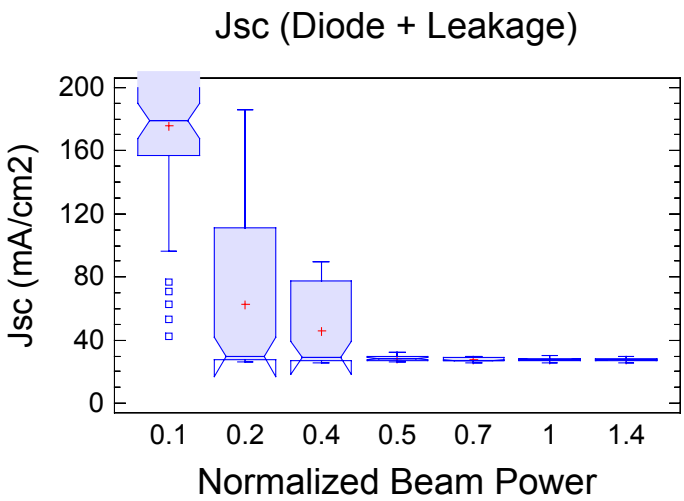

Figure 1.4 Indicated Jsc of small area devices isolated by laser scribing the front TCO contact at various beam power density settings

Ink jet reliability has been increased in Phase 3 through the elimination of clogging of small orifices. Prematurely dried adhesive in or near the inkjet dispense parts was identified and eliminated as one cause. Particulate contamination was identified as another cause of clogging, and was substantially eliminated through more effective cleaning and assembly procedures.

Anomalies in the volume of inkjet fluid at the start or end of a printed line, shown in Figure 1.5, have also been minimized.

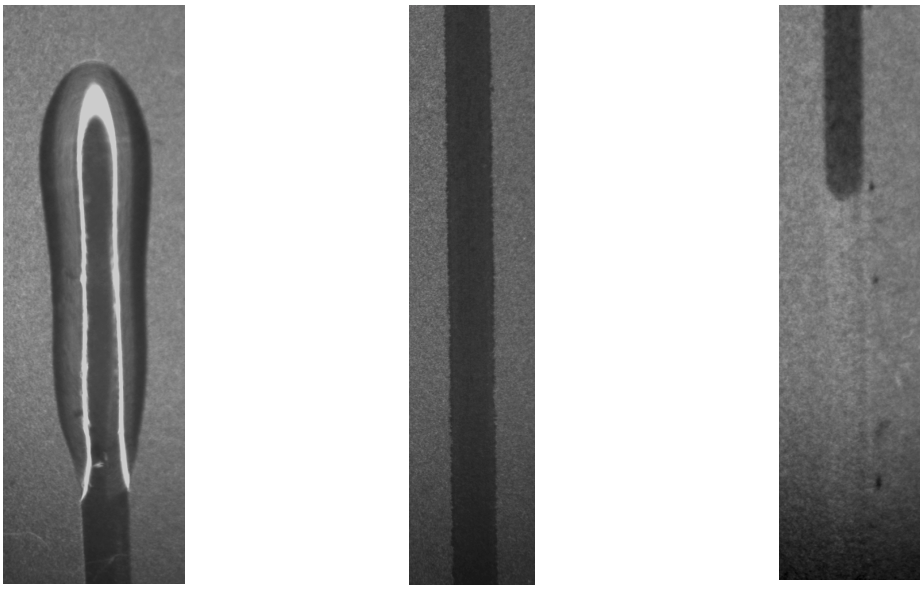

a b c

Figure 1.5 Optical micrograph showing the start (a) middle (b) and end (c) of an inkjet deposited line made using smaller dispense tip orifices. The linewidth in the region shown in the center image is 100 microns.

Relocation and modification of the ink valves resulted in a reduction in both actuation-deposition delay times and excess ink deposited at the start and end of scribes.

The result of these improvements has been that the number of sequential scribes that can be deposited without an inkjet problem has increased in Phase 3 from a range of 100-200 into the range of 3,000 to 10,000.

Increased Throughput

Although some increases in throughput were attained through software improvements, such as more efficient pattern generation, faster fiducial recognition, and automation of the alignment at the second laser operation, the large share of throughput increases were garnered incrementally through planned changes in the way the equipment was operated. In Phase 3, dual inkjet capability was installed after the existing inkjet design had reached an acceptable level of performance. Two inkjet heads were planned to match the capability of the four laser beams if two beams were used for back contact scribing and two were used for via scribe creation in the first laser operation.

Subsequently, the inkjet operation was demonstrated for bidirectional deposition across the web, depositing a cured ink line moving across the web in either direction. Bidirectional capability had been demonstrated prior to Phase 3 for all laser processes. Finally, a sequential process consisting of a discrete laser scribe patterning step followed by an ink jet print step for each module was merged into a single, integrated step in which the inkjet print using two heads was accomplished concurrently with the laser scribe using 4 beams (2 for back contact scribe and 2 for via scribe. Inkjet deposition was accomplished during the same patterning moves with the inkjet back-filling and curing immediately following the laser scribe cutting of the back contact.

Scribe Compression—Minimizing Total Area Loss

The Phase 3 PVMaT goal to minimize total interconnect widths to a level of 250 microns is critical in several aspects. Very small total interconnect widths result in a minimum of dead area loss in the module, enabling higher efficiency at the module level. For utility use and some space applications, high voltage module output is desirable and, again, is enabled by a greater number of very narrow module segments, which also require narrow interconnects. Narrow interconnects, in addition to allowing use of narrow module segments, relax the constraints on the front contact sheet resistivity and give greater design flexibility.

Much of what is required to achieve narrow interconnects is covered in previous sections as improvements in reliability and accuracy. Given a sufficient level of registration accuracy, between the individual laser scribes, the printed ink line, and the first and second laser operations, the total interconnect width would not be limited by spacing requirements.

As the developed laser scribes did not range beyond 70 or 80 microns in width, the strongest determinant of total interconnect width was the width of the printed ink line. Many variants and sizes of dispense tips were evaluated to minimize the printed ink line while maintaining reliability and line-width consistency, finally producing ink linewidths between 100 and 150 microns. Figure 1.6 below shows an SEM micrograph of a total interconnect that is about 240 microns wide, the culmination of these efforts.

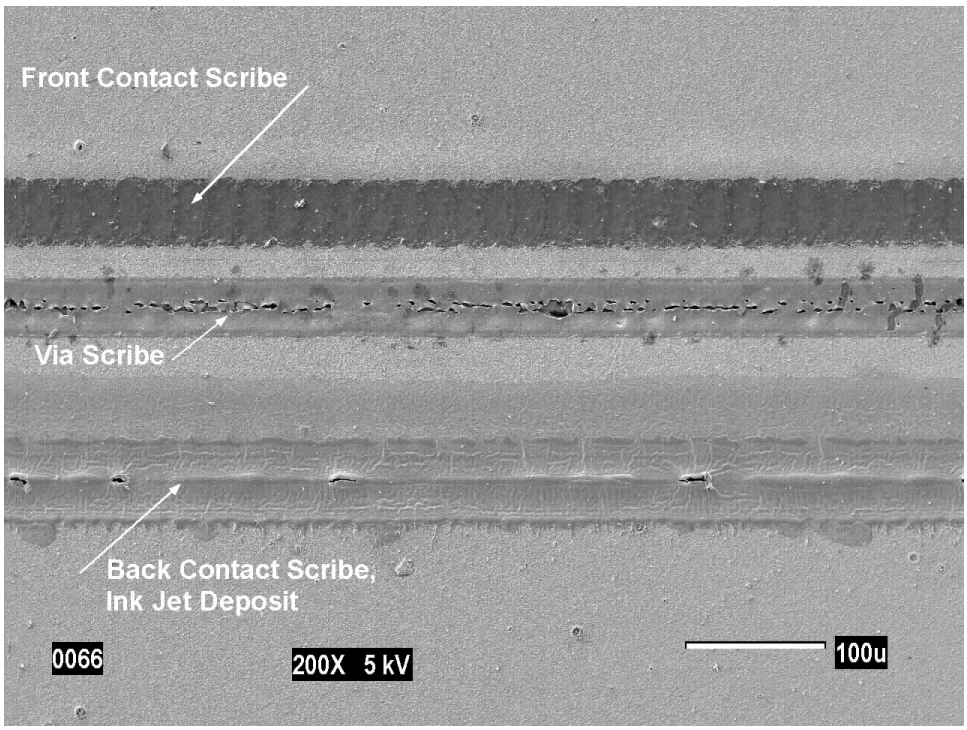

Figure 1.6 An SEM micrograph of a monolithic interconnect made on polyimide based CIGS using the GSE all-laser scribing and inkjet processes

Representative measurements taken at widely varying locations to evaluate total interconnect width at the start, middle, and end of large modules and from both left and right edges, indicate an average total interconnect width of 292 microns, with a standard deviation of about 30 microns. The distance between the scribes in the front and back contact (dependent only on laser operations) can be held to about 200 microns, with a standard deviation of 19 microns. The

largest variation occurs in the ink linewidth itself, with a standard deviation of 36 microns around an average width of 141 microns. The interconnects evaluated were done using full 4-beam, dual inkjet head, bidirectional operation with concurrent operation of the inkjet and the laser scribing in the first laser operation, all at a 12-in/sec scribing rate.

An example of the high voltage module capability enabled by such narrow monolithic interconnects is shown in Figure 1.7 below. That module design in a 32-inch x 12-inch format flexible, lightweight package produces over 300 volts open circuit.

Figure 1.7 A flexible, lightweight monolithically integrated CIGS module on polyimide in a 12-inch x 32-inch format having more than 300 volts output under outdoor illumination conditions

1.5 Summary

GSE has successfully developed a high speed, all-laser monolithic integration process for CIGS based modules on polyimide substrates. PVMaT goals for scribing rate and total interconnect width have both been exceeded. High voltage modules having a voltage output of more than 300 volts in a 32-inch x 12-inch format have been produced using the monolithic integration process. Despite the requirement for selective cutting of thin film layers, most of the individual process steps are tolerant, well-controlled and robust. Work remains to re-optimize the process

conditions for the via scribe subsequent to the adoption of an alternate back contact and some changes in the CIGS deposition parameters. Also, although total interconnect linewidths of less than 250 microns have been produced, greater control over the inkjet printing process is still required to attain the 250 micron linewidth on a more routine basis.

The processes and production equipment have been established for high speed processing of 13-inch wide polyimide product, and with capabilities that enable high efficiency, high voltage PV product.

1.6 Alternate Back Contact (Addendum)

As part of a continuing effort of the earlier PVMaT task to develop an improved back contact, we report here the successful substitution of an alloy-based back contact for the traditional molybdenum back contact. Several drawbacks exist for the molybdenum back contact. The material itself is expensive, but more importantly, molybdenum used as a back contact on polyimide is prone to microscopic crack formation. The cracking disrupts the electrical continuity of that contact, a crucial property responsible for efficient current collection. Microscopic examination indicated that both compressive and tensile cracking occur on the polyimide, but that the tensile failure is primarily responsible for the loss of electrical continuity. Tensile failure cracks in molybdenum are shown in Figure 1.8 and Figure 1.9 below.

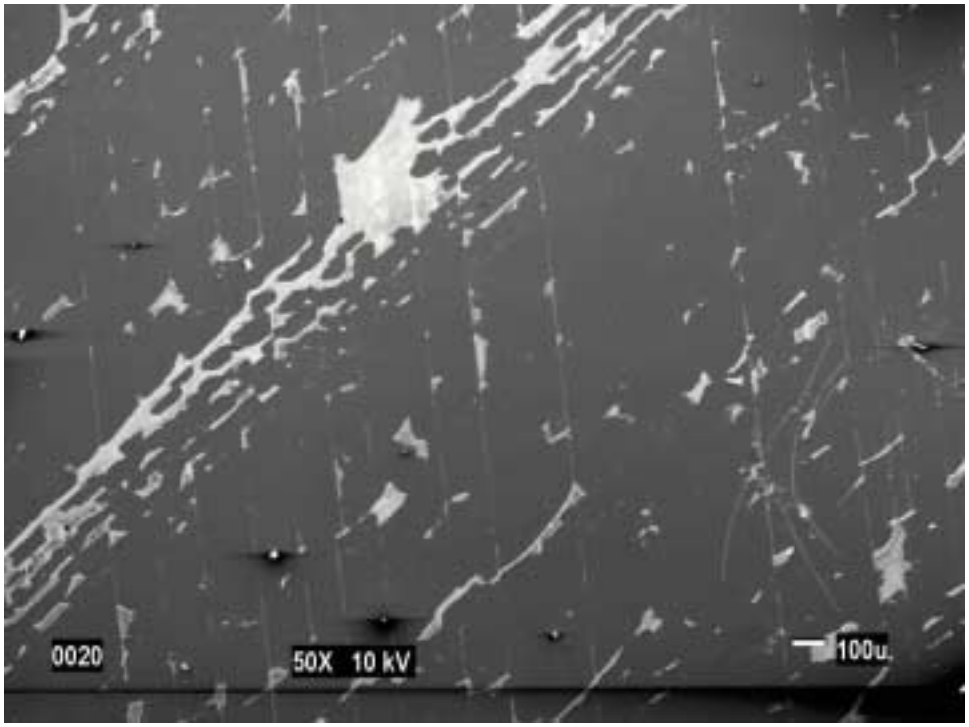

Figure 1.8 An SEM micrograph of cracks formed in the Mo back contact (CIGS absorber layer has been pulled off)

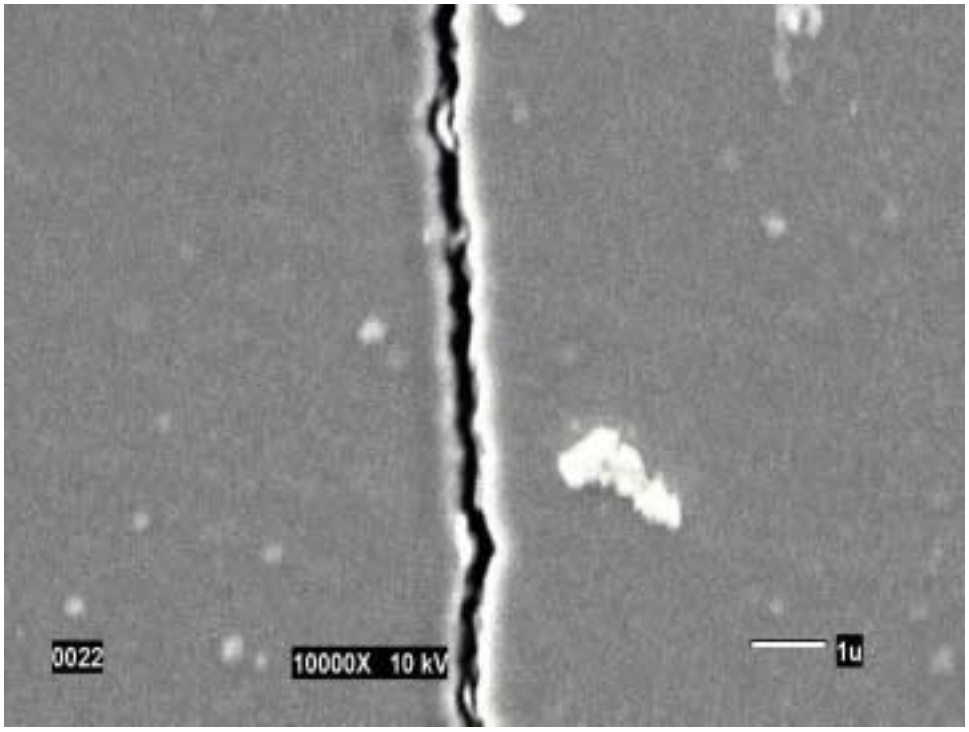

Figure 1.9 A higher magnification image of the cracks shown in Fig 1.8 above

The back contact cracking occurs during the highest temperature deposition steps, specifically during CIGS deposition. Several possible reasons exist for the cracking, not the least of which is that the Mo and the polyimide differ in coefficient of thermal expansion by a factor of 2.8. Also, the Mo is hard and brittle by nature, and typically exists with significant thin film stress after deposition by sputtering on the polyimide.

The alternate back contact is compared to a Mo back contact in Table 1.1. Sheet resistivity measurements, taken by a 4-point probe are among the most reliable indicators of back contact cracking. In the example cited in the table, the Mo back contact sheet resistance before CIGS deposition was about 0.5 ohms/square. The dramatic rise in sheet resistance after CIGS deposition is remarkable. Moreover, the sheet resistance typically becomes anisotropic, due to orientation of the cracks.

Table 1.1 Alternate back contact compared to a Mo back contact

	Sheet Resistivity (ohms/square)	
Contact/Direction	**Mean**	**Std. Deviation**
Mo / Across Web	182.2	65.5
Mo / Down Web	19.3	15.6
Alt. / Across Web	0.338	0.018
Alt. / Down Web	0.326	0.008

On the other hand, the alternate back contact was about 0.33 ohms/square prior to CIGS deposition. As shown in the table above, there is no significant change or anisotropy in the sheet resistance for the alternate contact after CIGS deposition. Although characterization of the back contact continues, GSE has now standardized the use of the alternate contact material for polyimide substrates.

2.0 Incorporation of High-rate CIGS Deposition

2.1 Introduction

One limiting factor for PV module throughput, and subsequent cost, is the absorber deposition. Neither the equipment nor the proof of concept exist for very high rate CIGS deposition for use in large area thin film PV manufacturing. The challenges in this task are the high rate, controlled, simultaneous delivery of Cu, In, Ga and Se to the substrate surface under conditions that form a dense, stoichiometric, well adherent film of high quality CIGS. Issues including control of the Ga concentration, as well as Ga concentration profile to control absorber bandgap, impurity and defect densities, morphology, grain boundaries and surface termination are all critical to absorber layer quality, and thus also to device and module performance.

For co-evaporation processes the kinetic rate limitation on CIGS compound formation is not known. Generally high quality CIGS has been formed at relatively slow rates (>30 min. deposition time). However, work in some laboratories using elemental co-evaporation at high substrate temperatures (>500 °C) indicates that a high quality CIGS absorber layer can be formed using 5-10 min. for the metals delivery [2-1]. High-rate deposition bodes well for a rapid manufacturing process, however, the manufacturing process used at GSE introduces several additional constraints. Large area, uniform deposition of CIGS must be accomplished at GSE with process temperatures less than about 400°C because higher temperatures degrade the flexible polymer substrate. Consequently, mixing and mass transport that are dependent on diffusion are much reduced compared to the diffusive rates that exist at much higher temperatures when CIGS is grown on glass substrates. Moreover, the intrinsic source of sodium associated with glass substrates is unavailable when using polymer substrates. Sodium incorporation has been shown to improve absorber quality and spatial uniformity of the photo response [2-2, 2-3]. The formation of CIGS at high rates, with low temperatures and on polymer substrates is unexplored.

Photogeneration and charge collection take place in CIGS absorber layer and so it is central to photovoltaic performance. Electronic properties such as carrier concentration and mobility, defect densities, minority carrier lifetime and internal electric junction field strength are critical. Along with the above-mentioned electronic characteristics, physical aspects such as adhesion and continuity of absorber coverage have dramatic effects on final module performance. The absorber deposition process must yielding high quality material, be economical, fast, controllable and scaleable to large area.

One additional consideration for manufacturable absorber processes is selenium utilization. Although excess of Se is provided in laboratory systems to enhance CIGS growth, a 3 to 4 times stoichiometric excess of Se for continuous operation of in-line CIGS systems may increase downtime for clean-up and costs associated with waste disposal.

2.2 Objectives

High-rate deposition of the absorber layer is essential to raise throughput and reduce manufacturing costs for thin-film PV. GSE is using large-area coevaporation of elemental

constituents in a continuous, roll-to-roll fashion to form the thin-film CIGS absorber. Key issues with CIGS deposition are:

- Design of evaporative sources capable of uniform, controllable, high-rate delivery of reactants over a large area
- Electronic quality and adhesion of CIGS deposited at high rates, within the constraints of a low substrate-temperature process
- Source heat dissipation to web and chamber
- Materials utilization, Se delivery and system maintenance and downtime

GSE is developing the equipment and methods for CIGS absorber deposition at high rates. Key goals of this task are to:

- Revise existing evaporative source designs capable of uniform, controllable, high-rate delivery of reactants over a large area
- Evaluate CIGS absorber quality at progressively higher deposition rates, up to 27 cm/minutes web speed (a 100 % increase over base rate)
- Develop methods for deposition of well-adherent, high quality CIGS at high rates and low substrate temperature
- Demonstrate module production using the high-rate process
- Incorporate high-rate absorber deposition methods and equipment into the GSE manufacturing line

2.3 Technical Approach

The baseline GSE CIGS manufacturing process consists of direct co-evaporation from elemental sources and was selected over sequential based sputtering processes because:

- Co-evaporation allows direct gallium incorporation into the active region of the absorber even at low substrate temperatures resulting in higher bandgap, and thus higher voltage per module segment.
- Substantially reduced cost because of high materials utilization (70 to 80% compared to 20 to 30% for sputtering) and low cost starting materials.
- Ability to produce quality stoichiometric and off-stoichiometric compounds (i.e., transition from Cu-lean to Cu-rich and back Cu-lean within a single deposition zone).
- Process throughput for direct co-evaporation is much higher because finishing heat treatments are not necessary, and capital cost for the required deposition equipment is significantly lower.
- Direct co-evaporation from elemental sources has higher materials utilization and avoids source material fabrication costs associated with making and bonding sputtering targets. These avoided costs and speed advantages take on extreme importance in a manufacturing environment.

- Compared to the elemental sputtering/selenization, direct co-evaporation has yielded CIGS material of better quality, evidenced by devices having higher efficiency.

For large-area, high-rate vapor phase manufacturing of compound semiconductor devices, multi-source evaporation on a moving substrate (flexible or rigid) provides the best combination of performance and low cost.

Source modeling was conducted to optimize materials utilization while achieving a uniform thickness across the web. Down web composition uniformity is achieved by the web movement through a well-defined deposition zone at a constant speed. Modeling indicated that high source utilization (>60%) required a relatively close source-to-substrate spacing.

GSE has designed and built continuous roll-to-roll CIGS deposition systems using multi-source co-evaporation in which substrate are transported above sources operated at a constant flux. With specific spacing between the sources, the web motion creates a controllable flux profile at the substrate. Using a GSE roll coating system, adherent, uniform, stoichiometric CIGS has been deposited that is single phase and has large grains.

2.4 Accomplishments

Effusion Source

During Phase 1, GSE went through several iterations of effusion source design for the metals deposition. Deposition trials were conducted on webs up to 100 feet in length in the production CIGS coater. Numerous analyses validated that adequate down-web coating uniformity of Cu, Ga, and In were achieved. However, repeatability was determined to be insufficient for cost-effective production. It was unclear at the conclusion of Phase 1 whether the insufficient repeatability resulted from anomalous effusion source behavior, operational procedures, interaction with parallel process steps (such as Se application), or a combination of these factors.

During Phase 2, repeatability was improved by additional effusion source design modifications and standardized operational procedures. As a by-product of these improvements, coated web lengths were increased to 450 feet in length without sacrificing compositional uniformity. Effusion source design modifications to enable higher effusion rates at lower applied powers were only partially successful. Deleterious effusion source behavior grew more pronounced with the new source design.

Many extreme requirements exist that critically affect source design, the most obvious being high temperature operation for extended periods of time, material flux delivery that is uniform and well controlled, and limited heat dissipation to surrounding parts. At GSE we have taken innovative approaches toward meeting all the requirements for operational sources. Multiple iterations of source design or modification followed by evaluation were required to meet all of the technical challenges. Some of the technical requirements of source design are mutually conflicting, thus compromises were made to satisfy design issues.

Composition uniformity down the web is determined by the effusion sources and their associated controls. In the production system, control is accomplished via XRF through effusion source temperature (see Task 13). For the control system to be effective, the effusion sources must behave predictably. Early in the GSE PVMaT program, anomalous behavior such as spitting and sudden increases in effusion rate made rate control difficult. For baseline CIGS runs at a web

speed of 6 inches/minute, the majority of the problems have subsequently been eliminated by minor modifications to the standard source design, improved maintenance and operational procedures.

Down web uniformity is best demonstrated across multiple lots. The composition and thickness control routinely achieved in the CIGS production chamber is summarized in Figure 2.1 through Figure 2.3 for five consecutive lots. Each lot is between 200-300 feet in coated length. Samples were removed down the web at equally spaced intervals for EDS analysis (20kV) of composition. CIGS thickness was determined from X-SEM on the same samples. The majority of these lots are well within the specification limits for Cu/(Ga+In) and thickness.

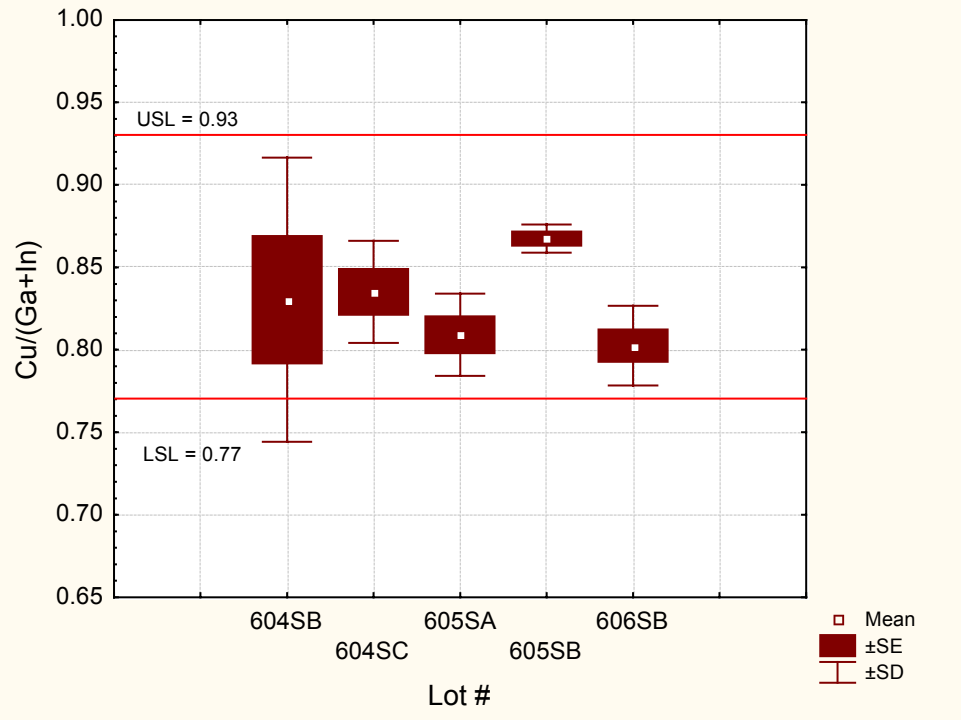

Figure 2.1 Cu/(Ga+In) by EDS (20kV) for five consecutive lots (center only)

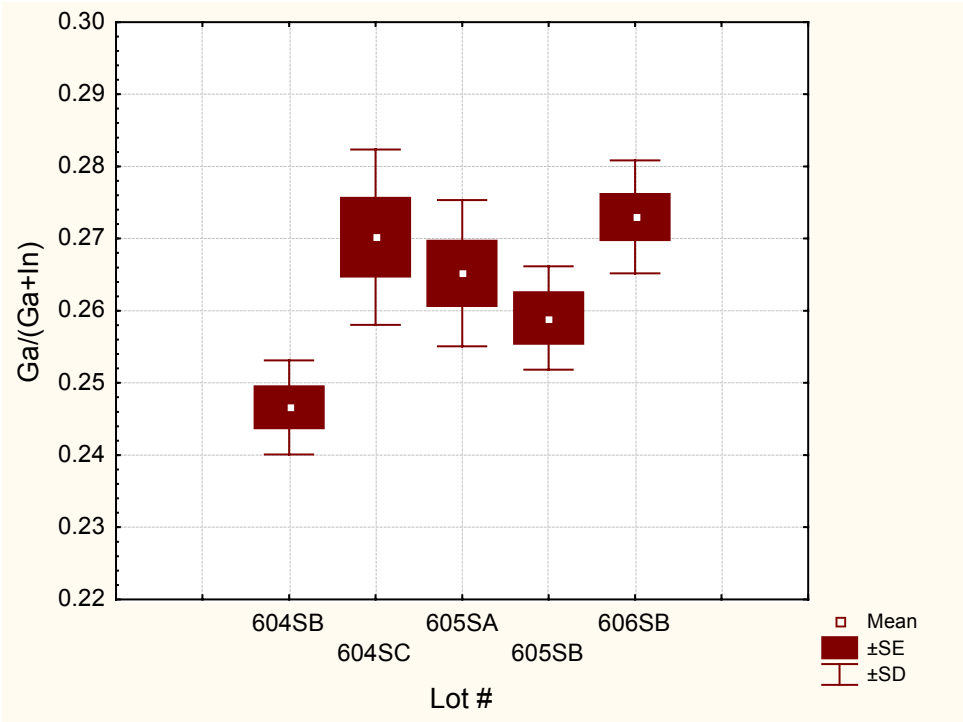

Figure 2.2 Ga/(Ga+In) by EDS (20kV) for five consecutive lots (center only)

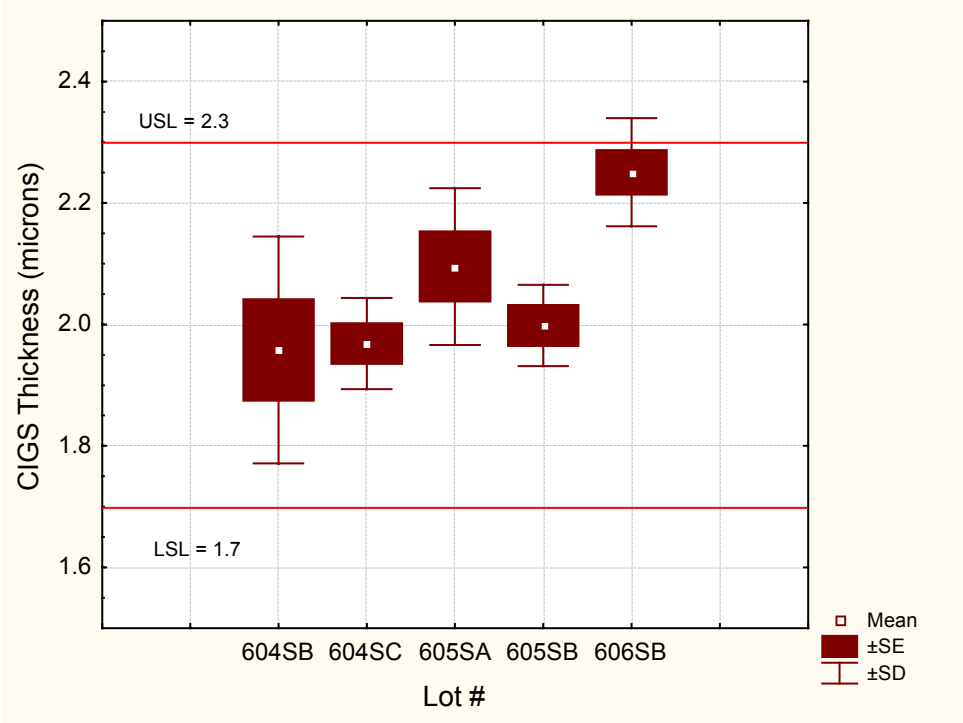

Figure 2.3 CIGS thickness by SEM x-section for five consecutive lots (center only)

The delivery efficiency and consumption rates of the metals have been tracked throughout the effusion source development program. After the numerous iterations in source design and process design and control, the delivery efficiency for Cu and In was determined to be between

40-45% (Table 2.1) for an analysis conducted across multiple lots. The consumption rates per unit web length for the metals appear in Table 2.2. Table 2.3 shows steady-state power consumption of effusion sources at program end.

Table 2.1 Cu and In delivery efficiency across multiple lots at program end

Metal	Lots	Mean	Minimum	Maximum	Std.Dev.
Cu	23	0.427	0.317	0.540	0.057
In	22	0.447	0.313	0.566	0.084

Table 2.2 Metals consumption rates at program end

Metal	Consumption Rate (g/100 ft.)
Cu	49
In	71
Ga	39

Table 2.3 Steady-state power consumption of effusion sources at program end

Source	Voltage (VAC)	Current (A)	Power (kW)
Cu	29	83.0	2.41
In	19	53.0	1.01
Ga	22	67.5	1.49

High-rate CIGS Deposition

During Phase 1, deposition trials were conducted in the CIGS production coater at web speeds up to 24 inches/min. Comparable test diode efficiencies were obtained at web speeds of 6 and 12 inches/min. Analysis of composition, microstructure, morphology, and impurities failed to detect significant differences between CIGS films deposited with web speeds between 6 and 18 inches/min.

Additional comparisons between efficiency and web speed were made during Phase 2. Statistical analyses were complicated by anomalous effusion source behavior at the higher effusion rates required at faster web speeds. The clean data that was generated implied little or no decrease in efficiency at web speeds up to 12 inches/min.

In a series of web speed tests conducted during Phase 3, it was observed that cross-web Cu/(Ga+In) uniformity became poorer at higher web speeds, as shown in Figure 2.4. No similar trend was observed in Ga/(Ga+In), as shown in Figure 2.5

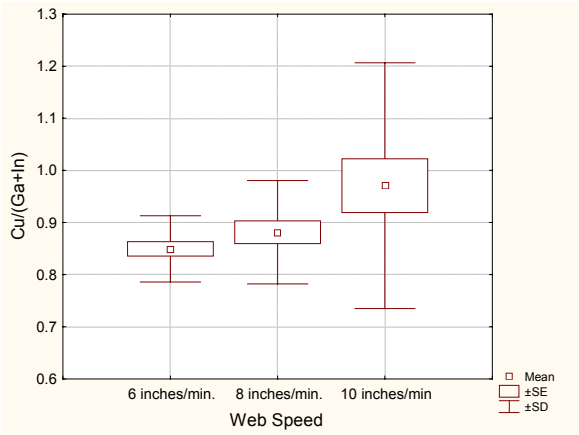

Figure 2.4 Cu/(Ga+In) uniformity at web speeds of 6, 8, and 10 inches/min.

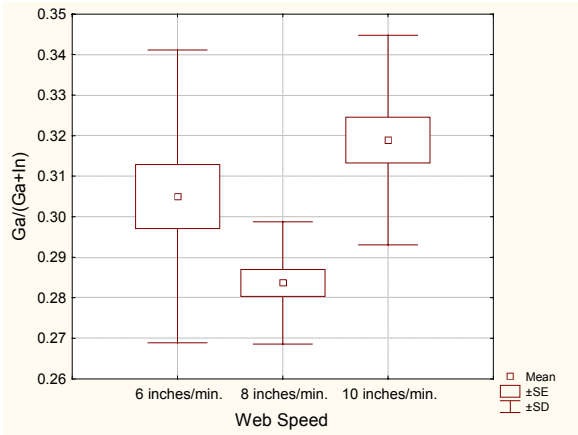

Figure 2.5 Ga/(Ga+In) uniformity at web speeds of 6, 8, and 10 inches/min.

The composition was characterized by EDS at 20kV on approximately 18 samples from across and along each web.

Closer examination revealed that cross-web non-uniformity of Cu was primarily responsible for the observed non-uniformity. The Cu effusion source operates at the highest temperature of all the sources, thus making it subject to larger thermal gradients. Large thermal gradients are expected to negatively impact the cross-web deposit thickness profile.

Although equivalent efficiencies have been demonstrated at higher web speeds, the application of higher web speeds requires additional engineering design modifications of the effusion source to guarantee that process specification limits can be met.

Se Consumption and Delivery

At the beginning of Phase 1, a Se delivery system was installed in the production CIGS coater that consisted of a single containment/heating assembly with a gas distribution manifold to enable uniform Se delivery throughout the deposition area. Se effusion rate was enabled by direct control of the Se melt temperature. A means for determining the consumption rate of Se from lot-to-lot by volumetric measurements was implemented and data tracking was initiated.

During Phase 2, multiple Se delivery systems were installed to allow independent control of Se effusion at different points in the CIGS deposition process. Tracking of consumption rate continued. Process tests were completed to determine the point below which Se starvation negatively impacted product performance. Significant run-to-run variation in Se consumption under nominally identical conditions was observed.

A decision to relocate the Se reservoir to a cooler location in the production CIGS coater was made early in Phase 3 based on the inadequate control determined during Phase 2. The decision was motivated by data that indicated better thermal control over the reservoir would improve control of Se delivery. At about the same time, variations in the In thickness as measured by in-situ XRF were correlated to fluctuations in the power applied to the Se reservoir to maintain it at a constant temperature. It appeared that In thickness on the web was either increased by higher effusion efficiency (due to an increase in mean free path at lower Se pressure) or decreased due

to volatilization of less-stable indium selenide species. With no direct measurement of Se effusion rate available, it was difficult to identify the mechanism responsible.

Tests were performed to determine if the temperature profile of the reservoir could be modified to minimize the impact on In thickness. Three heater configurations were selected and tested. The results, shown in Figure 2.6 through Figure 2.8, demonstrate the strong effect thermal gradients in the reservoir had on Se effusion rate. Configuration 3 was standardized after it was determined to be superior for allowing a more uniform In thickness.

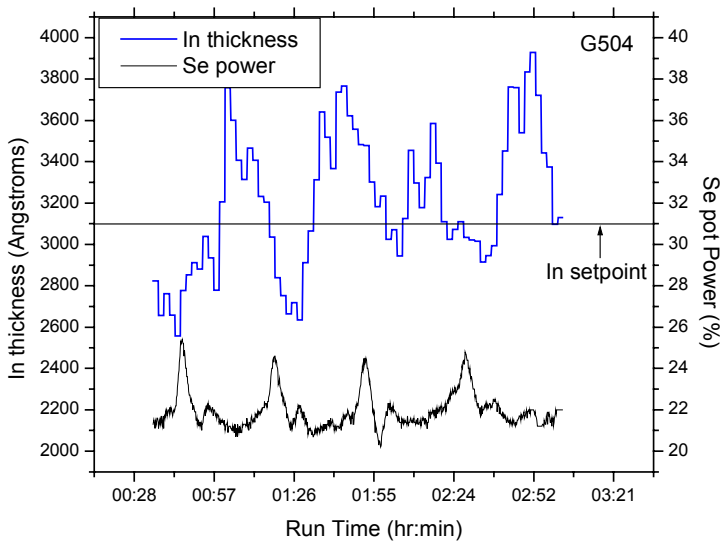

Figure 2.6 In thickness and Se pot power as a function of run time for heater configuration 1

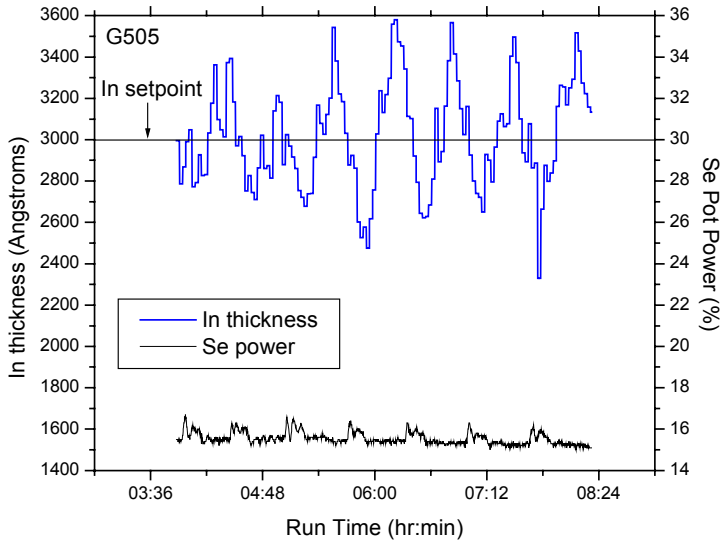

Figure 2.7 In thickness and Se pot power as a function of run time for heater configuration 2

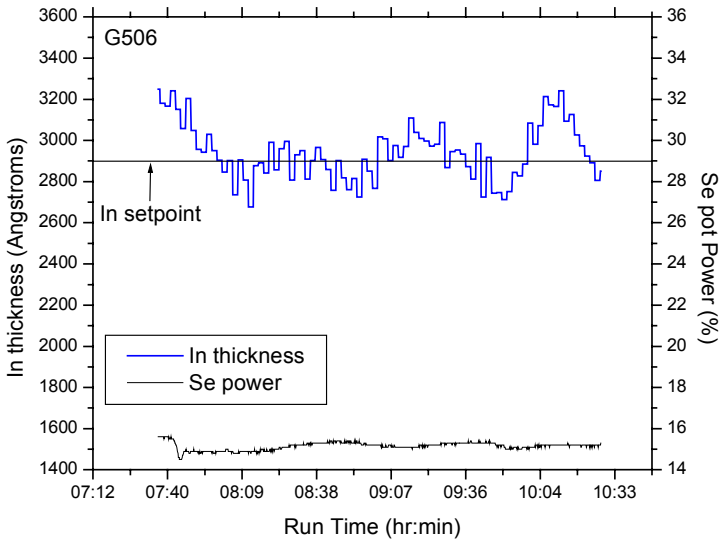

Figure 2.8 In thickness and Se pot power as a function of run time for heater configuration 3

Although the heater reconfiguration improved the apparent control, the variation that remained was still deemed too large to achieve the compositional control necessary for hi-yield manufacture. Without a direct technique for quantifying Se in the deposition zone, it was difficult to identify needed improvements to the Se delivery system. After an exhaustive search, a novel sensor was identified and then modified for application as a Se sensor.

After installation in the production coater, tests were conducted to correlate the Se sensor output to other sensor data for validation. The output from the sensor was correlated to variations in Se power and In thickness (Figure 2.9 and Figure 2.10). Monitoring the output for a period of time and comparing it to the Se reservoir temperature led to an approximate operating range for the sensor. During this continuous testing, the sensor was found to be both repeatable and robust in the harsh chamber environment.

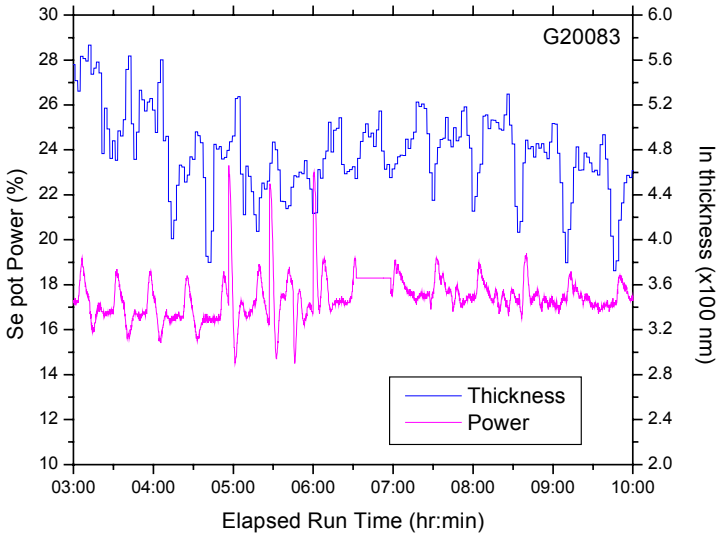

Figure 2.9 Se pot power and In thickness as a function of elapsed run time

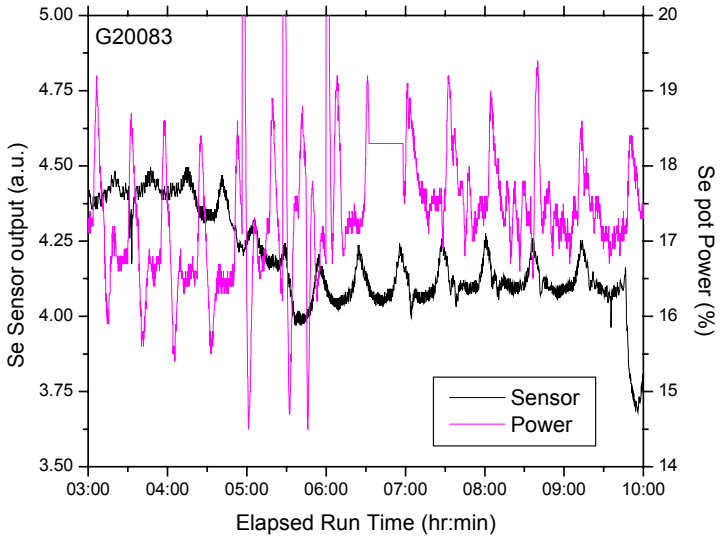

Figure 2.10 Se sensor output and Se pot power as a function of elapsed run time

After validating its utility, the Se sensor was integrated into the production chamber control platform and architecture. An appropriate set of control algorithms was developed and incorporated into the control logic.

With the aid of the sensor, inherent flaws in the design and operation of the Se delivery system were identified. Primary problems determined were: corrosion and subsequent blockage of the system components; inadequate heating of critical components in the system, thus promoting condensation and blockage; and control interactions between separately heated components of the Se delivery system.

A variety of materials in the delivery system were tested for improved corrosion resistance. None were found that substantially increased the mean time between failure. Efforts were also made to eliminate cold spots in the delivery system. Although condensation was eliminated, blockage due to corrosion became problematic at the higher temperatures. In addition, transient start-up conditions frequently filled the delivery system with molten Se before the sensor detected any Se. Control was impossible once this condition occurred.

A radical re-design of the delivery system was made once the failure mechanisms were identified. Minor problems were identified in the re-design and quickly eliminated. After tuning the entire system, excellent control of Se was demonstrated (see Figure 2.11). Replicate systems were installed in additional locations in the production CIGS coater. As a result of tighter Se control, In thickness control improved dramatically, as illustrated in Figure 2.12.

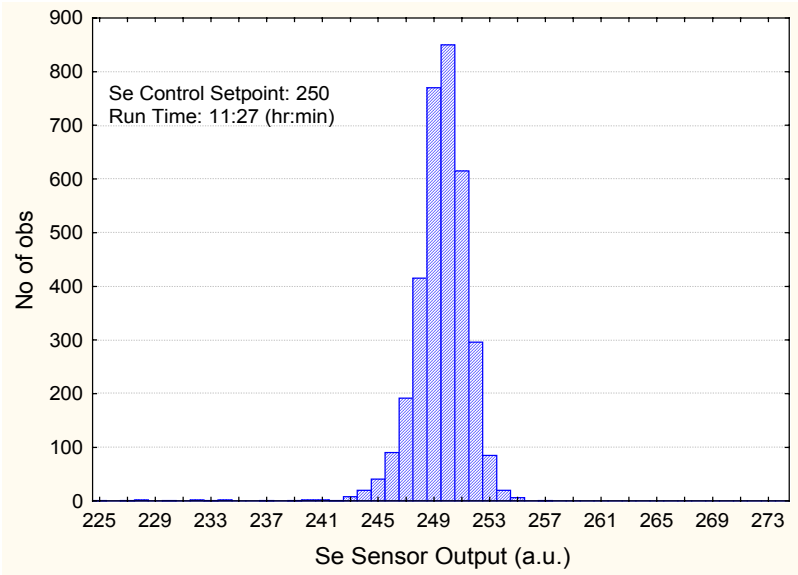

Figure 2.11 Histogram of Se control response (506SA)

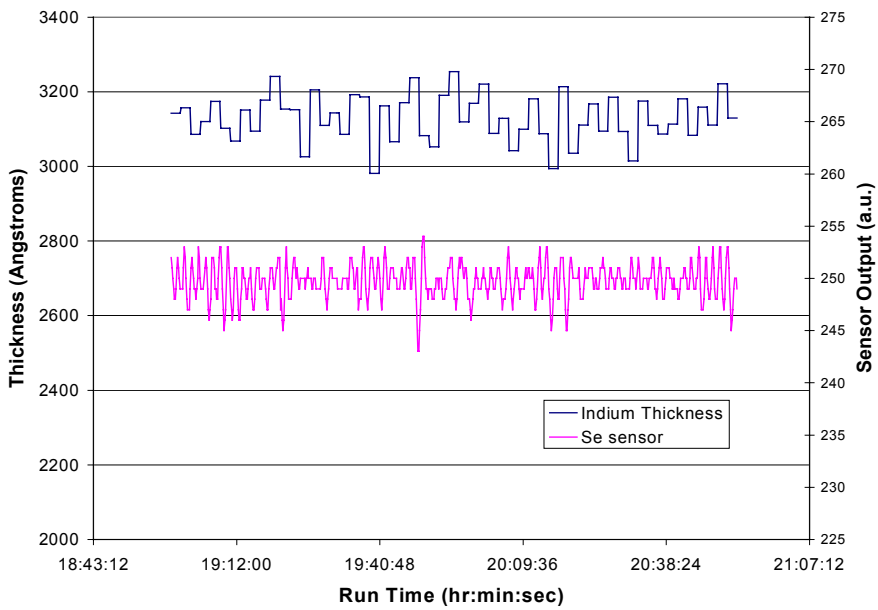

Figure 2.12 In thickness and Se sensor output as a function of run time (517SA)

A number of tests were conducted using DOE methodology after gaining control of the Se. The rapid response and accurate control of Se enabled by the redesigned system facilitated the test process. An example of the control possible appears in the logged test data from a DOE run (Figure 2.13).

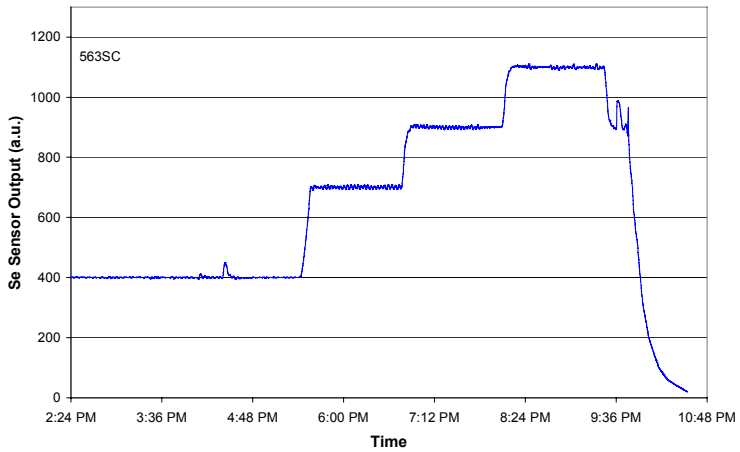

Figure 2.13 Se control response demonstrated during a DOE run

A Se/metals ratio of 3-5 is generally considered ideal for CIGS deposition in a laboratory bell jar. The onset of Se starvation was identified in the production CIGS coater by correlating device parameters to the Se control set point during the CIGS coating process. After optimization, the amount of Se necessary to make efficient diodes was determined to be substantially less than expected. The application of a ratio as low as 1.3 yielded device efficiencies that were equivalent to ratios greater than 2 in the GSE production system (Table 2.4). Confinement of the Se in the deposition area likely allows greater Se utilization.

Table 2.4 Selenium utilization and average diode efficiency for two consecutive lots

Lot	Effusion Rate (g/min.)				Se/Metals (Molar ratio)	Avg. Diode Efficiency (%)
	Cu	Ga	In	Se		
605SA	0.250	0.225	0.287	1.133	1.49	9.7
605SB	0.273	0.275	0.351	1.175	1.32	8.9

Se consumption rate data gathered before and after the system re-design are further testimonial to the improved control (Figure 2.14). Se consumption is determined from the difference in the Se reservoir weight before and after a deposition run, normalized to the length of web coated during the run. Prior to the re-design, the mean Se consumption was 513g/100 ft. Afterwards, the mean consumption was 197g/100 ft., a decrease of 62%.

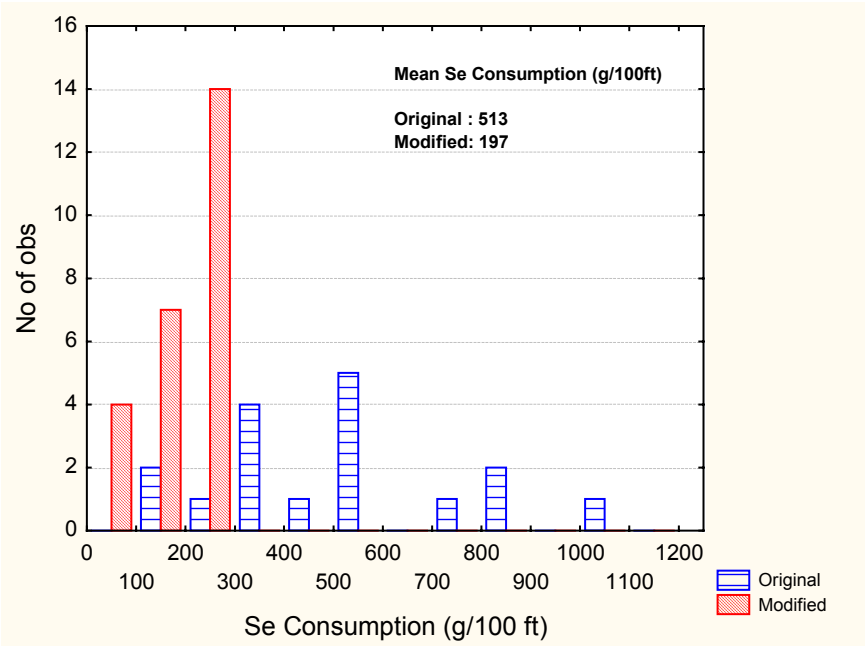

Figure 2.14 Se consumption rate before and after the delivery system redesign

2.5 Summary

At GSE we have been successful in developing methods for high rate deposition of high purity CIGS using a low temperature, roll-to-roll process on flexible substrates. CIGS deposited in continuous roll-to-roll process is of good quality, as indicated by device results, even at substrate rates that exceed the PVMaT end-of-contract goal. The aspects of this task associated with the highest risks (scaled-up evaporative source design and very high rate CIGS formation) have already been attacked, with good result. Deposition of CIGS by co-evaporation at very high rates over large areas appears to be viable, but additional engineering improvements to the effusion source are required before a high yield, high-rate process can be incorporated into the GSE production line. The effusion source improvements made under the PVMaT program have directly increased yield and output power at a web speed of 6 inches/min.

Se utilization has been substantially improved during the program duration. A huge benefit to process control and repeatability has been realized as a by-product of this development.

3.0 Realtime, Intelligent Control of CIGS Deposition

3.1 Parallel Detector Spectroscopic Ellipsometer (PDSE)

Introduction

Fundamental mechanisms underlying processing and materials performance relationships in more complex and dynamic thin-film structures may not be revealed in post-processing measurements. For these cases, effective feedback process control is critical and underscores the need for real-time measurement and interpretation of system parameters. Although process models and simulators enable development of effective process reactor designs and model-based control strategies, real-time sensing and control of critical process and product variables is required to accommodate unanticipated process upsets, reactor variability/drift, and perhaps allow operation in physically unstable processing regimes where repeatability can be achieved only through dynamic feedback/feedforward control.

For in-situ, real-time thin film property measurements, it has been particularly useful to concentrate on the polarization state of light reflected from deposited films, and how this is modified through the interaction with the sample. A spectroscopic ellipsometer (SE) sensor was developed to measure several thin-film properties simultaneously, such as thickness, morphology, and resistivity, and provide the real-time sensing required for effective CIGS process control. Unlike conventional ellipsometers, which measure the intensity of the reflected polychromatic light for each polarizer orientation, our SE utilizes carefully selected polarization states (intensities) to determine complex reflectance and/or ellipsometric amplitude (Ψ) and phase (Δ).

The amplitude and phase change parameters (Ψ, Δ) obtained in ellipsometry can also be expressed in terms of the changes upon reflection in the angular orientation and ellipticity of the polarization ellipse associated with the incident wave. Unlike a reflectance measurement, which only provides the ratio of reflected to incidence irradiances, an ellipsometer can extract both real and imaginary parts of the dielectric function, (ε_1,ε_2), as a function of the photon energy, ($h\nu$), from the (Ψ,Δ) measurement.

In addition to spectroscopic ellipsometer, X-ray Florescence (XRF) was also developed as a complementary technique for providing in-situ CIGS film composition and thickness analysis. By monitoring the florescence spectrum from the CIGS film being illuminated by x-rays, specific film composition is obtained by carefully determining peak energies and overall size and shape in the spectra. This provides a reliable method for determining the amount of each element in the film and thus the total thickness of the film and relative elemental ratios.

Objectives

Diagnostic tool development is necessary to enable real-time control during the absorber deposition for the extended times necessary to process up to 1000 feet of substrate. Cost and yield improvements resulted from better control of the CIGS properties in the roll-to-roll process. The key issues with intelligent control of the absorber layer deposition included:

- Demonstrating sensitivity of the diagnostic methods to key electronic and physical CIGS properties.
- Demonstrating sensor robustness, reliability and suitability to in-situ deposition conditions.
- Developing algorithms for data reduction to provide meaningful and predictive output with speed for real-time operation.

To meet these objectives, a Parallel Detector Spectroscopic Ellipsometer (PDSE) and an X-ray Florescence (XRF) system were developed to provide real-time, in-situ film property measurements for intelligent process control. The key goals of this task included:

- Demonstrating that the PDSE and XRF methods were sensitive to and predictive of the crucial electrical and physical properties of the CIGS absorber material.
- Designing and installing practical PDSE and XRF equipment on production equipment.
- Developing robust, practical algorithms to reduce raw data to information that is uniquely predictive of the important electronic and physical qualities of the CIGS.

Technical Approach

As discussed above, the ellipsometer is a unique technique in that the real and imaginary parts of the dielectric function can be extracted directly as a function of photon energy. For the homogeneous, layer-by-layer growth of a perfectly uniform transparent or absorbing film on an ideal, fully characterized substrate, real-time ellipsometry at single photon energy has been shown to provide the dielectric function of a film along with its thickness. The dielectric function, $\varepsilon(\omega,K)$, which describes the response of a material to an electromagnetic field has significant consequences for the physical properties of a solid. It depends sensitively on the electronic band structure (and other physical properties) of a material and studies of the dielectric function by optical spectroscopy (multi-frequency response) are very useful in the determination of a material's overall band structure.

Several spectroscopic ellipsometry systems have been designed for in-situ process monitoring. Some can be purchased as an integrated device. However, there are no spectroscopic ellipsometers currently available (either commercially or in any reported development laboratory) that acquire all of the necessary information in a single, rapid sampling; nor are these systems cheap. Since no spectroscopic ellipsometer with appropriate capabilities is commercially available, we developed a novel Spectroscopic Ellipsometer sensor for in-line, real-time control of CIGS manufacturing processes. The SE sensor we developed has the potential of measuring several thin-film properties simultaneously, such as thickness, band structure, and morphology, and providing the real-time sensing required for effective CIGS process control (spectroscopic data can now be acquired in parallel over a wide photon energy range in less than 50 ms).

Accomplishments

The assembly of an operational PDSE system was completed in the fall of 1999. Testing of the PDSE to acquire calibrated data and to be able to realign to maintain the calibration was also completed in Phase 2. The PDSE acquired data with as much or more accuracy and precision as a state-of-the-art analytical spectroscopic ellipsometer. A calibration procedure was defined that

is flexible enough to allow changes based on materials and other geometrical concerns that might arise once the PDSE is installed in the production CIGS chamber. Once the initial ex-situ testing was performed with the PDSE, it was installed and operated in a prototype CIGS vacuum deposition chamber. The PDSE provided real-time, in-situ SE measurements in vacuum conditions to 10^{-6} torr with the external and internal optical and electronic components at 70ºC. Using the results of this initial in-situ testing, a design was been finalized and construction began on the PDSE hardware that was installed in the 15 inch web production CIGS vacuum deposition chamber.

Spectroscopic ellipsometry measurements and analysis was performed on thirteen CIGS samples provided by IEC. Initial modeling of the measured data proved to be very challenging but indicated that SE can provide the type of film property information that will be needed for real-time process control. Besides all the film property information that can be obtained from a detailed evaluation of the SE measurements, the initial data analysis indicates that we may be able to use the "raw" real-time data to provide information about the film quality, the bandgap (and thus the composition) and the surface roughness. Based on these initial results, transformation algorithms were developed in Phase 3 to convert the SE data to quantified information for process control. Ultimately, a next generation, 'smart' interpretive algorithm(s), may be developed and applied to the CIGS processes that can provide additional information about the film properties, but this will require a significant increase in the present research and development effort. In either case, both approaches will need to be validated for the CIGS deposition process.

PDSE Hardware Development

While the Phase 2 effort to design, construct and install a functional PDSE into a research reactor was successfully completed, several outstanding hardware development issues remained to be resolved. The main issues included substantially enhancing the computer control and software platform, increasing the signal to noise, developing a better understanding of the calibration process, developing a more robust alignment procedure, and developing true parallel IR collection capabilities. Initially, a PDSE control platform using HPVee software was written to perform several of the required data collection processes for the PDSE hardware. However, significant limitations involving driver availability for some PDSE components and poor support forced us to rewrite the PDSE control platform using the more versatile and better supported Labview software. This new Labview based control platform software provides complete control of all PDSE functions including both multiple visible and IR spectrometer operation, alignment actuator control, alignment algorithm incorporation, calibration instrument matrix and data regression calculations, and data output and active real-time data monitoring.

Angular Alignment Sensitivity

In addition to control platform improvements, several tests were performed to improve light throughput, primarily by determining the specific effects of diffusers on alignment sensitivity and light collection. One of the design challenges of the PDSE has been balancing the angular sensitivity of the detection head alignment with the intensity throughput for each channel. Initial attempts to focus the beam directly on the optical fibers leading to the spectrometer gave suitable intensity with an 8-Watt lamp, but made the PDSE extremely sensitive to alignment. After performing experiments to determine a suitable solution, a diffuser plate between the condensing lens and the optical fiber was used to sufficiently reduce the alignment sensitivity. However, the

"cosine" diffuser plates, initially used, scattered the light in a 180-degree solid angle, decreasing the amount of light collected by the optical fiber by over two orders of magnitude. A 200 to 1000-Watt Xe arc lamp was used to increase the collected signals with intensities near the range needed for analysis. While increasing the input lamp power provides reasonable signal to noise for measurements from smooth samples, measurements from rougher and non-ideal samples like CIGS can decrease the signal to noise by 1 or two orders of magnitude. Increasing incident lamp power an additional one or two orders of magnitude becomes problematic due to the heat and light carrying ability of the optical fibers and the availability and price of sources with 10,000 or 100,000 W outputs that have the correct geometries to efficiently couple to optical fibers. Therefore, optimization of the diffuser-optical fiber collection coupling was investigated to determine if detected light throughput could be increased while angular alignment sensitivity was minimized sufficiently. The two main areas that were investigated involved systematic study of other diffusers that have smaller scattering solid angles and study of optical fibers with larger apertures.

Experimental Set-up

An experiment to quantitatively measure the change in collected intensity as a function of incident angle (angular sensitivity) used a rotating optical stage with accuracy to 30 arc-seconds, a visible region spectrometer, a fiber optic mount with a 5 mm focal length lens and an 8-Watt quartz halogen lamp. The 8-Watt lamp provided light to the incident optical fiber that was mounted to an optical table. The detector assembly, that included a focusing lens and the collection optical fiber, was mounted on the rotating optical stage with the collection lens at the center of the rotation. The diffuser was placed at the focal point of the collection lens in the detector assembly and had the standard optical fiber ~6 mm from the diffuser or the optical fiber taper ~ 2 mm from the diffuser.

While a larger optical fiber diameter does reduce angular alignment sensitivity and increase light collection, the maximum fiber diameter is limited by the bend radius needed and the commercial availability of the fiber, i.e. cost. The use of a fiber bundle was investigated early on, but was limited by the individual acceptance angles of the individual fibers and the fact that it transported the angular sensitivity to the other end of the fiber bundle. Furthermore, while a fiber taper increases the surface area for the light to hit, the acceptance angle is decreased significantly. For example, light collected by a 2 mm to 1 mm diameter fiber taper in the configuration used for these experiments was approximately the same as the 1 mm diameter optical fiber by itself. Angular deviations of the incident light on the lens are Fourier transformed into linear translation in the focal plane. The concept behind using a fiber taper is to provide a large enough area so that the linear translations of the light fall completely within the optical surface and are collected with the same efficiency.

Angular Sensitivity and Intensity Comparison of Tapered-end Fiber and Standard Fiber (No Diffuser)

The use of a 1 mm to 2 mm diameter fiber taper in place of the standard 1 mm diameter optical fiber was investigated. The results are presented in Figure 3.1 and indicate that both optical fibers had a similar angular dependence and in fact the fiber taper had lower collection efficiency. The latter is most likely related to a poorer polish on the 1 mm fiber ends.

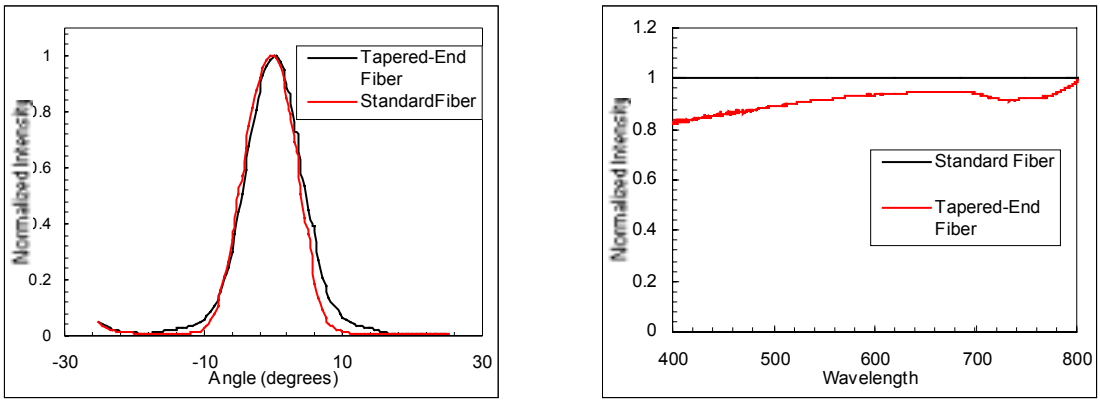

(a) (b)

Figure 3.1 Angular (a) and intensity (b) comparison of a standard 1 mm diameter optical fiber and 1 mm to 2 mm diameter fiber taper

Comparison of Angular Sensitivity for Various Diffusers

The standard "cosine" diffusers that were initially used in the PDSE sufficiently decrease alignment sensitivity but significantly decrease the amount of light collected. Alternative "elliptical" diffusers are commercially available with coatings that are adjusted to a defined amount of solid angle scattering. A 10 degree and 80 degree elliptical diffuser was used in place of the cosine diffuser with the standard 1 mm diameter collection optical fiber and the 2 mm diameter taper fiber. The intensity versus incident angle was measured for each diffuser and compared to the results with the cosine diffuser (Figure 3.2). The elliptical diffusers with the 1 mm diameter optical fiber (Figure 3.2-a) and the 10 degree elliptical diffuser with the 2 mm fiber taper did not sufficiently reduce the alignment sensitivity. However, the 80 degree elliptical diffuser in conjunction with the 2 mm fiber taper provided approximately the same decrease of alignment sensitivity as the cosine diffuser for incident angles between +/- 5 degrees (Figure 3.2-b). Beyond +/- 5 degrees, the angular sensitivity of the 80 degree elliptical diffuser with the fiber taper was significantly higher than the standard diffuser/ optical fiber arrangement (Figure 3.3-a).

While the angular sensitivity of the 80 degree elliptical diffuser with the tapered-end fiber is approximately the same as the standard diffuser within +/- 5 degrees, the intensity collection is increased close to an order of magnitude. Figure 3.3-b compares the collected intensities of the 80 degree elliptical diffuser with the tapered-end fiber arrangement with that of the standard diffuser/optical fiber arrangement.

The angular sensitivity of the standard diffuser is unmatched by either the taper fiber alone or the use of holographic elliptical diffusers. Over a small range of angles (five degrees either side of center), however, the combination of the 80 degree elliptical diffuser with the tapered-end fiber provides nearly the identical angular sensitivity with an order of magnitude increase of intensity throughput. Therefore it should be possible to use the 80 degree elliptical diffuser with the tapered-end fiber with the PDSE to obtain better signal to noise without significantly increasing sensitivity to angular deviations within the detection head.

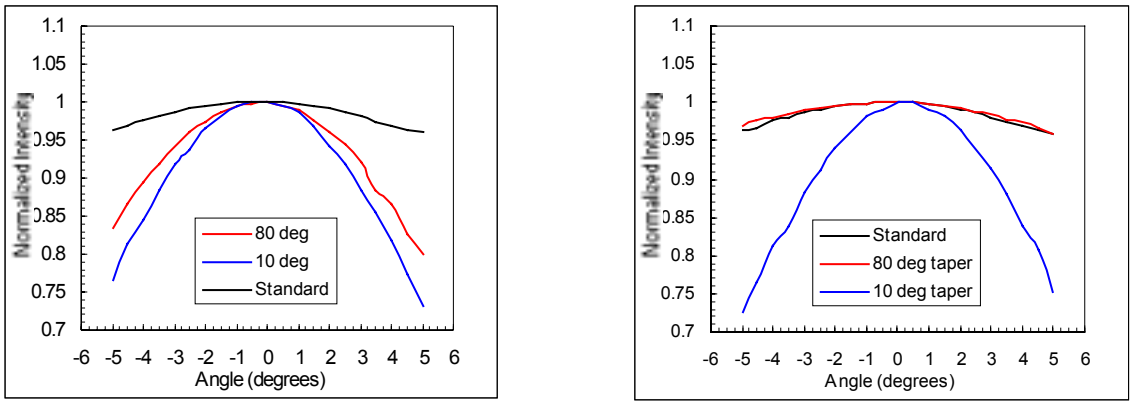

(a) (b)

Figure 3.2 Measured angular dependence of an 80 degree elliptical, 10 degree elliptical and standard cosine diffuser with a 1 mm diameter optical fiber (a) and a 2 mm fiber taper (b)

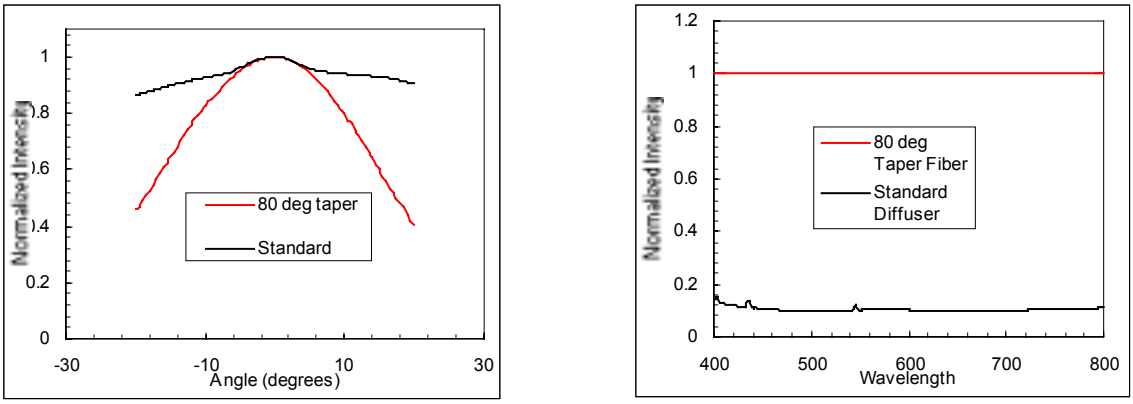

(a) (b)

Figure 3.3 Angular sensitivity of 80 degree elliptical diffuser with 2 mm fiber taper and standard diffuser/ optical fiber over a 40 degree span (a), and normalized throughput intensity comparison between 80 degree elliptical diffuser with fiber taper and standard diffuser/ optical fiber arrangement (b)

While the experiment described above provided a baseline from which to evaluate the angular sensitivity of the diffuser/optical fiber system, the main issue is the relationship of angular sensitivity on the spectroscopic ellipsometry data. Thus a systematic set of tests were performed to determine if the 10 degree diffusers or no diffusers could be used to collect spectroscopic ellipsometry data without adversely affecting alignment sensitivity (Figure 3.4). The data indicate that the 10 degree diffusers provide substantially more signal to noise compared to the 80 degree diffusers and significantly decreases alignment sensitivity compared to the not using diffusers.

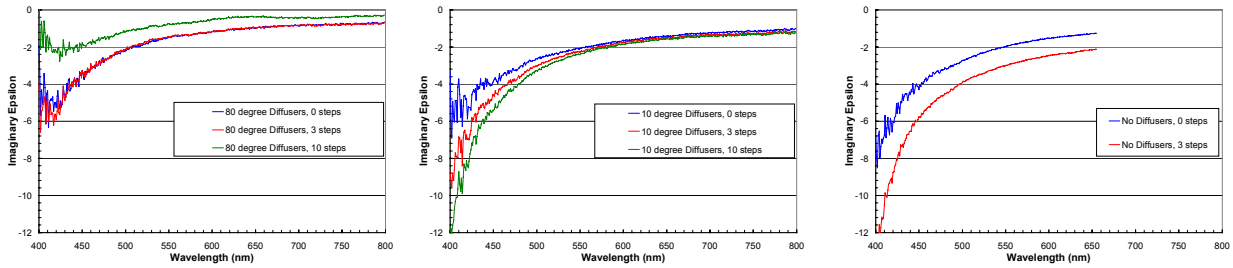

(a) (b) (c)

Figure 3.4 Measured angular dependence of PDSE data from Si with 80 degree elliptical (a), 10 degree elliptical (b) and no diffuser (c). The data indicate that the PDSE has the least alignment sensitivity with the 80 degree diffusers and the greatest with no diffusers. Furthermore, the data indicate that the 10 degree diffusers provide a good compromise between the two by substantially increasing signal to noise while decreasing alignment sensitivity.

PDSE IR Capability

Previously, ITN's PDSE system used four Ocean Optics spectrometers in a "master/ slave" configuration that permitted simultaneous measurement from four spectrometers. Unfortunately, these Charged-Couple-Device (CCD)-based spectrometers only operate between 250 and 850 nm. ITN had also previously purchased two Zeiss near IR (NIR) spectrometers that operate between 940 and 1720 nm. Ideally, four IR spectrometers are needed for PDSE measurements of the CIGS bandgap and transparent regions. However, a multiple IR spectrometer system is presently not commercially available. Unlike the visible CCD-based spectrometers that are commercially available in multiple spectrometer configurations that allow simultaneous data collect from all four spectrometers, the available IR spectrometers can only be operated one at a time with commercially available software drivers and configurations. For this effort, ITN worked with Zeiss and TechBase 5 to develop the drivers that allowed simultaneous measurement from the two Zeiss NIR spectrometers. This required procurement of new software drivers, new hardware PCI-based electronics, and new software development performed at ITN to simultaneously operate multiple IR spectrometers. Figure 3.5 shows the spectra obtained simultaneously from two IR spectrometers. With the successful demonstration of simultaneous operation of two IR spectrometers, two additional IR spectrometers were ordered at the beginning of the Phase 3 effort to complete the demonstration of simultaneous data collection from four IR spectrometers that will allow PDSE data to be collected in a few milliseconds. Unfortunately, due to government regulations, the hardware and software components of the four IR spectrometer systems did not arrive until the end of Phase 3. In the interim, to obtain experience and demonstrate feasibility of an IR PDSE, an optical switch was designed and constructed that precisely realigns the four optical fibers from the PDSE with an optical fiber on a single IR spectrometer. Figure 3.6-b shows the initial testing results of an operation optical switch (shown in Figure 3.6-a).

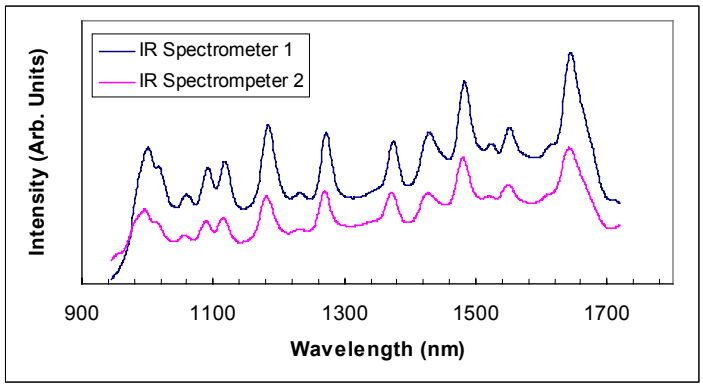

Figure 3.5 Spectra simultaneously collected by two IR spectrometers

While the optical switch has only limited functionality for obtaining "real-time" data in our present reaction chamber that uses a continually moving web, it will be available for use in applications where the samples can be stopped for a short time and only one IR spectrometer is economically feasible. Furthermore, the optical switch provided the ability to collect calibrated PDSE data from Si and CIGS/Mo thin deposited films on flexible stainless steel substrates (Figure 3.6-b) and successfully demonstrated the ability of the PDSE to collect data in the IR from PV materials.

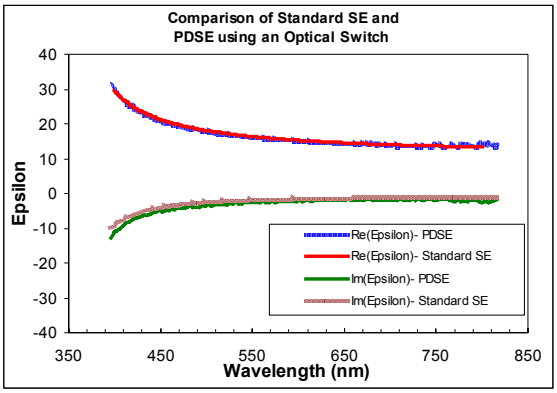

(a) (b)

Figure 3.6 An optical fiber switch was designed and constructed to collect four PDSE polarization states with one spectrometer (a), and comparison of data collected from Si with a standard SE and the PDSE using an optical switch and one spectrometer (b)

Once the additional IR spectrometers were delivered, addition software programming and testing was performed to operate four separate IR spectrometers simultaneously. This effort resulted for the first time in simultaneous operation of four IR spectrometers (Figure 3.7) to collect the four polarization states necessary to completely determine the film properties of a sample between 940 and 1720 nm in a few milliseconds. With four simultaneously operating IR spectrometers, data was collected in real-time as a CIGS sample moved across the PDSE detection system (Figure 3.8). The data indicate that the PDSE provides a very sensitive measurement of film properties that can easily distinguish angstrom level film thickness and optical property differences.

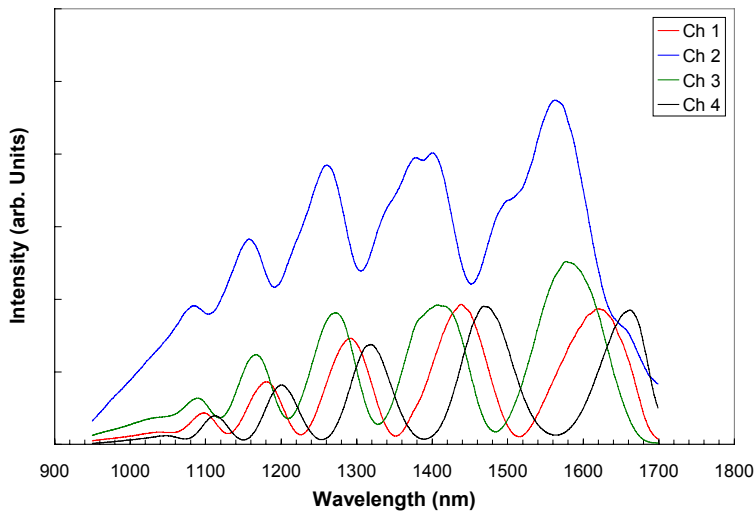

Figure 3.7 **Simultaneously measured IR spectra from four PDSE channels. This represents the first time that complete polarization state information was collected using four IR spectrometers simultaneously.**

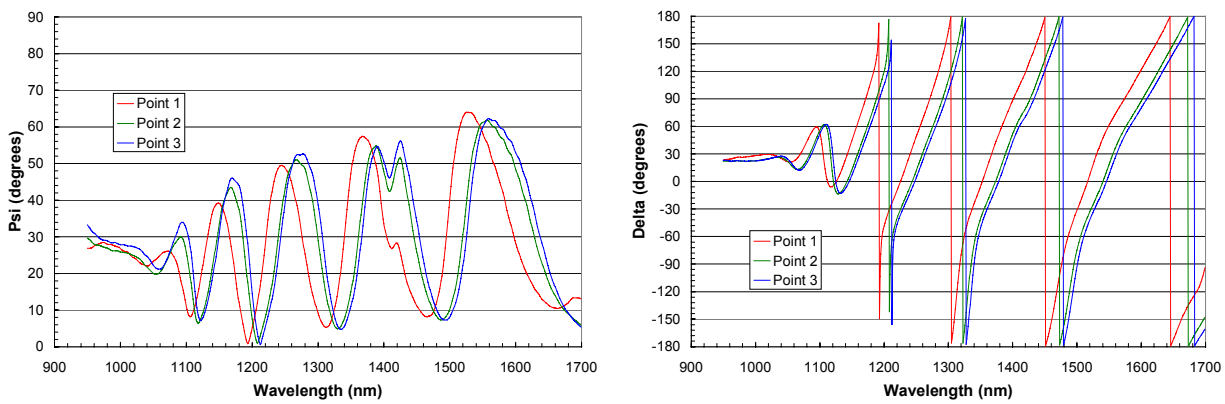

(a) (b)

Figure 3.8 **Measured CIGS ellipsometry data using the PDSE with four IR spectrometers to simultaneously collect four polarization states. The data were collected in real-time as the CIGS sample moved past the PDSE detection system. The slight shift in the data along with slightly different shapes indicates that the PDSE is very sensitive to film thickness (possibly on the order of a few angstroms resolution) and other optical and electronic film properties that are present even in a very good CIGS sample.**

PDSE Alignment and Calibration

While an initial set of alignment and calibration procedures were used to demonstrate the initial capabilities of the PDSE, two major factors remained to be resolved. The first issue involved the fact that the initial alignment process that used crossed laser beams and quadrant photo-diodes to provide information about the quality of the alignment was not sensitive enough to ensure alignment reproducibility to the degree needed for the PDSE. Thus the spectroscopic ellipsometry measurements were much more sensitive to alignment than the quadrant photo-diode measurements. The second issue involved the inability to consistently obtain a reproducible calibration, even though with a given calibration and calculated instrument matrix,

the PDSE produced very reproducible measurements. To resolve these two issues, a detailed set of tasks and experiments were performed to determine the causes and to find adequate solutions.

Alignment

Systematic alignment routines, based on maximizing total intensity in all four channels, were tested with and without a depolarizer. Initially, we had identified the use of a depolarizer to provide equivalent intensities to all four polarization state channels and then optimize the intensities in all four channels to define a reproducible alignment. This approach was proven initially with a PDSE detection head and then proven to a limited degree with an entire PDSE system. However, an adequate mathematical strategy could not be obtained that could be used to identify the direction of misalignment and then intelligently identify how to regain alignment. Furthermore, the depolarizer creates a wavelength dependent interference pattern in the PDSE spectra that hampers calibration. To aid with the alignment investigations, a versatile Labview program was written that identifies specific alignment conditions and provides the operator with quantifiable measures of alignment. The use of this alignment routine based on maximizing intensities provides better and more reproducible calibrations but the PDSE still remains very sensitive to alignment.

To further increase alignment reproducibility at both the fine and course levels, a robust alignment methodology was investigated that utilizes multiple color filters geometrically arranged to provide information about the location of the white light beam. The goal is to use the individual spectral signatures of each filter to determine which quadrant the white light beam is in and thus autonomously determine which direction to move to regain alignment. This filter along with an intensity maximization strategy may be sufficient to unambiguously determine when the PDSE is aligned. Additional work will be performed to ascertain the usefulness of these color filters for alignment and to develop a robust alignment methodology that can be performed autonomously by a computer.

Calibration

An initial set of systematic calibration and alignment experiments indicated that the PDSE calibration issues were not associated with the first collection lens, polarizing beam splitter orientation, or the path lengths to the optical fibers. Thus it appears that specific orientations of optical components in the detector head are not substantially contributing to calibration or alignment difficulties. Furthermore, the use of depolarized light to equilibrate intensities to each spectrometer did not seem to help, especially with the introduction of an interference pattern in the spectra. However, since the PDSE calibration was not able to remove the interference pattern as it should have, spectral differences between the four detectors were investigated. Initial recalibration of the spectrometers, assigning specific wavelengths to specific pixels uniformly in every spectrometer, also did not substantially improve the calibration results.

By far, the main component to attain a reproducible and good calibration involves obtaining a good and reproducible alignment. In addition, a significant source of calibration variability involved the temperature sensitivity of a quarter wave retarder Fresnel Rhomb. The rhomb displayed a phase shift change in excess of 30% with less than a 30-degree change in temperature. This temperature difference should have resulted in less than a 0.07% change in phase shift. While the specific cause of this temperature sensitivity is not known, the near term solution has been to use a PID controlled heater to maintain the temperature of the detection head

to within a degree. Additional solutions to this problem will be investigated. In addition to alignment and rhomb temperature sensitivity, other issues that were identified as potential problems for calibration include quarter wave plate alignment, acceptance lens alignment, and low signal collection in one or more channels during the calibration.

The main focus of this effort was to identify a methodology to provide reproducible and accurate PDSE calibrations. The identification of the temperature dependent rhomb along with the other issues have resulted in defining a calibration methodology that provides very reproducible results. The main issue is to provide sufficient alignment to obtain a reasonably accurate calibration.

PDSE Hardware Installation in CIGS Production Deposition Chamber

The PDSE designed and constructed for installation into CIGS-1 was completely assembled and tested with accompanying alignment system. The new alignment system that used optical fiber conduits to transport the light for the alignment system in and out of the vacuum deposition chamber and completely removed all electronics to the outside of the chamber was successfully operated. With the completion of the alignment system, a specific mounting system for the CIGS-1 chamber, and CIGS-1 chamber modifications, a PDSE was successfully installed and operated in the CIGS-1 production chamber for the first time. Data from the moving stainless steel web was collected in-situ while the chamber was under vacuum. The results from this initial set of tests indicated that wrinkles in the stainless steel web significantly misalign the optical path of the PDSE beam, requiring autonomous alignment capabilities to track the web orientation changes.

The wrinkles are related to tension control issues in the roll-to-roll manufacturing process, the flexible stainless steel web does not flow perfectly across the rollers. Small “wrinkles” occur as the web moves along the rollers due to thermal stress differences in the thin stainless steel sheets. While most of the material remains flat against the roller, during a significant amount of the time, a wrinkle causes part of the stainless steel web to lift off the roller. Since the PDSE relies on the web remaining flat against the roller, these small wrinkles creates a significant misalignment that reduces the amount of accurate measurements from the PDSE, even though the web does return to the original alignment once the wrinkle has past the roller. During the times when the PDSE was well aligned and a wrinkle was not present in the web, in-situ data from the moving stainless steel web was collected while the chamber was under vacuum and actively depositing CIGS thin films. The data shown in Figure 3.9 indicates that the PDSE accommodates vibration as the web moves and provides accurate thin film property measurements. Thus, for Phase 3, the PDSE was installed in a CIGS roll-to-roll deposition chamber and operated on a day-to-day basis to obtain valuable information in an operational deposition system and to gain experience and a database for CIGS samples.

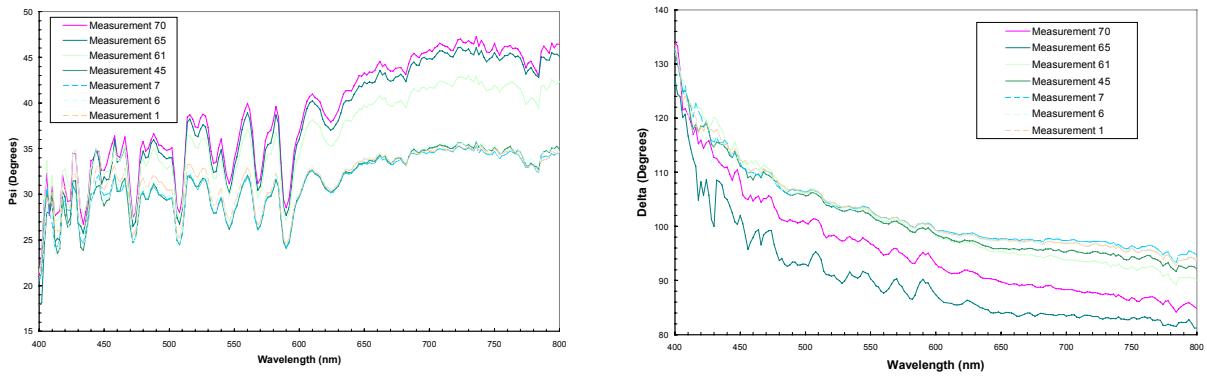

Figure 3.9 In-situ real-time PDSE data acquired from a moving flexible stainless steel substrate. While the PDSE accurately corrected for vibration, defective wrinkles in the substrate caused misalignment that could not be corrected for with the present alignment system. The data indicate that once the wrinkle passes the PDSE, the original alignment is regained and the measurement is again accurate.

PDSE Algorithm and Process Control Demonstrations

As part of our effort to demonstrate process control with PDSE measurements, an effort was performed to develop interpretive algorithms for process control using actual data from moving substrates. Several CIGS data analysis approaches were investigated, including a methodology that transformed the data into Fourier space for determining the bandgap and a simple methodology to predict film thickness. By transforming the data to Fourier space, the collective characteristics of the wavelength-dependent spectra are connected with localized features in an effective wavenumber-space. This provides a valuable method of classifying the raw data. Once this has been accomplished, the wavelength-dependent decay of the amplitude of the oscillations can be used as an identifier of the onset of absorption. A dielectric function interpolation routine to generate what should be the best estimate for the true optical properties of CIGS above the bandgap as a function of the In/Ga ratio was also being investigated. This interpolation routine depends upon knowing the location of the bandgap for a particular stoichiometry, a quantity that has been well-documented in the literature (also as a function of Cu concentration). Other critical points were linearly extrapolated between CIS and CGS. The approach to understanding the ellipsometry data on CIGS concentrated on extracting the best physical model for a given concentration, since the optical properties were fixed.

While these more complex interpretive algorithm methodologies provide intrinsic insight, reduction to real-time data interpretation is a daunting task. Furthermore, the simplest methodologies provided significant information with extremely fast computational analysis. For example, by using a simple relationship between the measured oscillations, in for example delta, the thickness of the CIGS films were quickly measured by simply determining the periodicity of the data (Figure 3.10-a). The slight shift in the data shown in Figure 3.8 indicates that the PDSE is extremely sensitive to thickness changes. By measuring the oscillation periodicity, we are easily able to monitor and quantitatively measure thickness on a moving CIGS film to within a few angstroms.

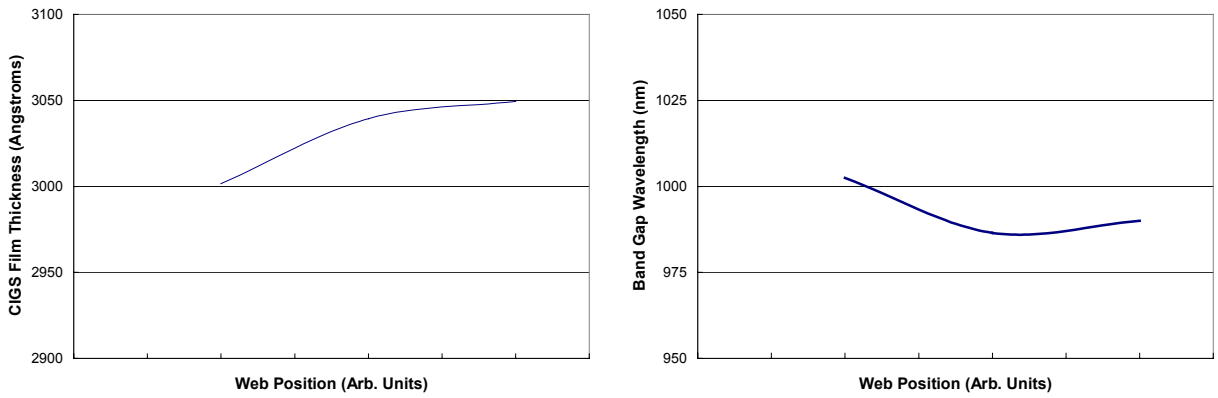

(a) (b)

Figure 3.10 Film thickness (a) and band gap (b) calculated with real-time processing interpretive algorithms from data measured as a CIGS thin film is moved passed the PDSE

In addition, by simply calculating the point at which the second derivative of the imaginary part of the pseudo-dielectric function becomes zero, i.e. a measure of the beginning of the CIGS absorption region, we can quickly and easily measure changes in the band gap energy in real-time as the CIGS material moves (Figure 3.10-b). The data in both figures demonstrate the capability of the PDSE to perform in-situ real-time CIGS film property measurements on a moving web, and demonstrates the ability of simple interpretive algorithms to provide useful information for process control.

Summary

The PDSE was successfully integrated into a production CIGS deposition chamber, providing in-situ real-time film property information in the harsh deposition environment that contains volatile Se species, heat, and vacuum conditions as low as 10^{-6} torr. The PDSE successfully collected data from continuously moving CIGS films on flexible substrates. Web vibrations did not significantly influence the optical measurements, however, wrinkles in the web induced significant misalignment, which will require adaptive and rapid realignment methodologies be employed to ensure the PDSE is properly aligned. However, the PDSE was able to provide useful measurements when the intermittent wrinkles were not present. Furthermore, interpretive algorithm methodologies were developed that provided thickness and band gap information about the CIGS film for real-time process control. Additional efforts included alignment and calibration sensitivity investigations and optimization.

3.2 X-ray Fluorescometry (XRF)

Background

XRF measurements are performed by illuminating a portion of a sample with x-rays and measuring the energy and count rate of the fluoresced x-rays. Since each element fluoresces at characteristic energies, the count rates at each energy can be used to extract composition data.

Hardware Installation

The XRF hardware installed in the GSE production CIGS coater was developed under a Thin Film Partnership Program subcontract (ZAK-8-17619-08). Novel features of the hardware include protection of the sensor from the deposition environment, use of a sensor-to-sample distance appropriate to deposition chambers, and the use of only low-cost components operating at room temperature. Novel aspects of the XRF analysis include one-sample calibration that gives valid results over a wide range of compositions, real-time CIGS analysis, and compensation for variations in substrate location and x-ray tube current drift by using the substrate signal. The application of XRF to CIGS deposition allows the use of innovative hardware and analysis because the elements present in the film are known prior to measurement, 1% precision is sufficient, and recent advances in x-ray tube and detector manufacture have occurred.

The sensor was installed on a roll-to-roll CIGS deposition system at Global Solar Energy, L.L.C. (GSE). The sensor was installed approximately 60" after the deposition zone, as was most convenient for the given chamber geometry. As currently designed, the XRF sensor can be exposed to Se flux and 200°C temperatures, but not to higher temperatures or to Cu, In, or Ga fluxes. Operation in the presence of vibrations larger than 0.01 g's is also unacceptable.

Control Strategy

Multiple effusion sources are utilized in the GSE CIGS deposition process. Separate effusion sources are utilized for each element and each source has a unique spatial location. Previous tests have shown that periodic corrections to the source temperature are required to maintain a constant effusion rate. The rate of required temperature set point changes is slow enough that composition sampling by XRF downstream from the deposition zone is sufficient for closed-loop control. The long delay between actual deposition and XRF measurement necessitates a two-stage controller.

The XRF sensor is used to estimate the effusion source temperature drift and predict the temperature set point needed to achieve a desired thickness, while a faster temperature controller around the effusion source thermal system maintains the temperature. The controller counteracts the drift by subtracting an estimate of the drift. A proportional output control is added to increase robustness to system variations. The control system was designed and implemented using a state-space representation and was assumed to be linear.

Accomplishments

A representative production run controlled by the strategy described above was conducted (517SA). The deposited web length, excluding the warm-up/pre-deposition phase, was approximately 330 feet. The web speed was six inches per minute, for a total deposition time of 660 minutes. The software control was activated at the beginning of the deposition. XRF thickness control set points for Cu, In, and Ga were 2000Å, 3000Å, and 1250Å, respectively.

The thicknesses of Cu, In, and Ga measured in-situ by the XRF during the deposition process are shown in Figure 3.11. The critical composition ratios Cu/(Ga+In), Ga/(Ga+In) calculated from the measured thicknesses are shown in Figure 3.12. The ratio Cu/(Ga+In) measured by XRF is slightly higher than that generally considered optimum, 0.85 - 0.90. We have determined

empirically that there is an offset between XRF and EDS derived ratios; the XRF ratios are generally 10% higher than the EDS ratios. The discrepancy between the two measurement techniques will be eliminated in the future through software modification with additional calibration.

The temperature set point changes to the Cu, In, and Ga sources derived from the control algorithms are shown in Figure 3.13 and Figure 3.14.

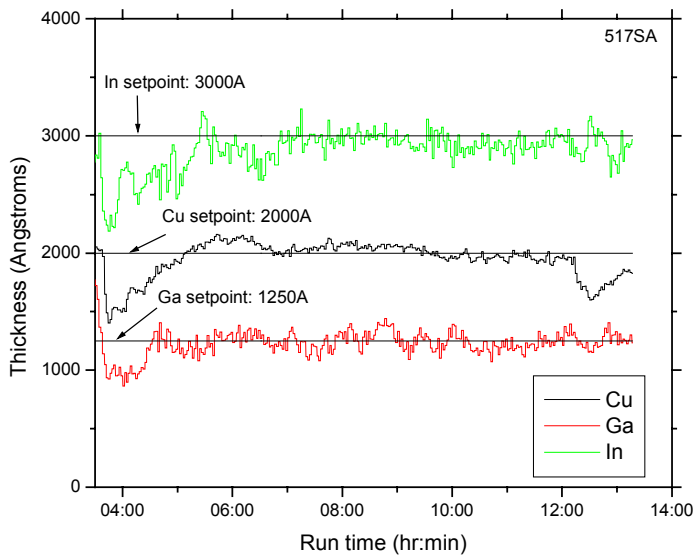

Figure 3.11 Elemental thicknesses of Cu, Ga, and In measured by XRF during a 315-foot deposition conducted under XRF feedback control

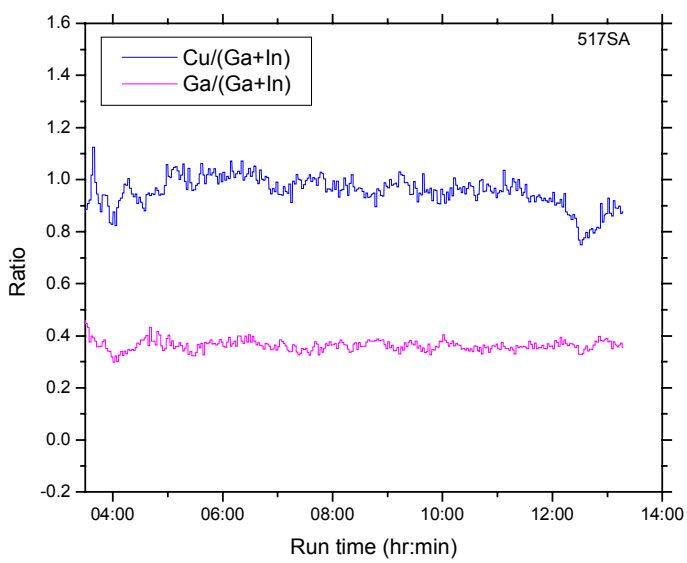

Figure 3.12 Composition ratios for the same deposition

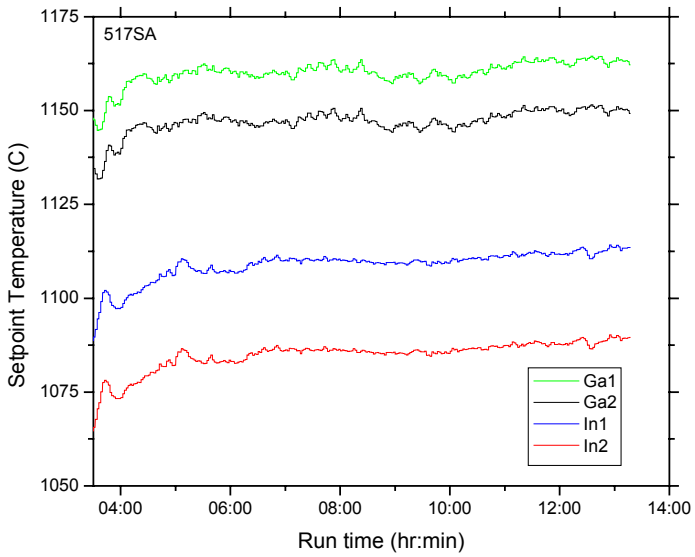

Figure 3.13 Temperature set point changes for Ga and In sources under XRF control

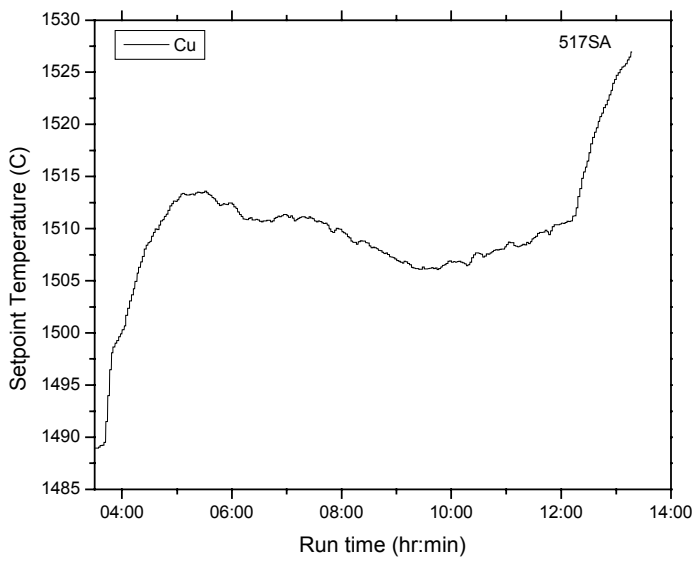

Figure 3.14 Temperature set point changes for the Cu source under XRF control

Summary

The XRF sensor is a robust tool with good reproducibility in an extreme environment. With XRF, excellent control of composition and thickness has been demonstrated in the production CIGS chambers. The XRF sensor and control strategy have been successfully integrated into all CIGS production chambers, and have contributed substantially to increased module yield and efficiency in the GSE production line.

4.0 Conclusions

The GSE production line has made marked improvements under the PVMaT program:

- Successfully developed a high-speed, all laser monolithic integration process for CIGS based modules on polyimide substrates
- Exceeded PVMaT goals for scribing rate and total interconnect width
- Developed robust, well-controlled techniques for selective scribing
- Improved CIGS evaporation sources to allow uniform, controllable delivery
- Completed foundation required to integrate higher CIGS deposition rates into the production line
- Developed well-controlled Se delivery system to minimize Se consumption
- Successfully integrated the PDSE into a production CIGS deposition chamber
- Collected useful, in-situ data with PDSE
- Validated the performance of the XRF sensor in the production CIGS deposition chamber
- Successfully incorporated the XRF sensor into the control architecture of the production CIGS deposition chamber.

REPORT DOCUMENTATION PAGE

Form Approved
OMB NO. 0704-0188

Public reporting burden for this collection of information is estimated to average 1 hour per response, including the time for reviewing instructions, searching existing data sources, gathering and maintaining the data needed, and completing and reviewing the collection of information. Send comments regarding this burden estimate or any other aspect of this collection of information, including suggestions for reducing this burden, to Washington Headquarters Services, Directorate for Information Operations and Reports, 1215 Jefferson Davis Highway, Suite 1204, Arlington, VA 22202-4302, and to the Office of Management and Budget, Paperwork Reduction Project (0704-0188), Washington, DC 20503.

1. AGENCY USE ONLY (Leave blank)	2. REPORT DATE April 2002	3. REPORT TYPE AND DATES COVERED Final Technical Report, July 1998 – September 2001

4. TITLE AND SUBTITLE
Photovoltaic Manufacturing Cost and Throughput Improvements for Thin Film CIGS-Based Modules, Final Technical Report, July 1998–September 2001

5. FUNDING NUMBERS
CF: ZAX-8-17647-11
PVP26101

6. AUTHOR(S)
J. Britt

7. PERFORMING ORGANIZATION NAME(S) AND ADDRESS(ES)
Global Solar Energy, L.L.C.
5575 So. Houghton Rd.
Tucson, Arizona 85747

8. PERFORMING ORGANIZATION REPORT NUMBER

9. SPONSORING/MONITORING AGENCY NAME(S) AND ADDRESS(ES)
National Renewable Energy Laboratory
1617 Cole Blvd.
Golden, CO 80401-3393

10. SPONSORING/MONITORING AGENCY REPORT NUMBER
NREL/SR-520-32072

11. SUPPLEMENTARY NOTES
NREL Technical Monitor: Richard L. Mitchell

12a. DISTRIBUTION/AVAILABILITY STATEMENT
National Technical Information Service
U.S. Department of Commerce
5285 Port Royal Road
Springfield, VA 22161

12b. DISTRIBUTION CODE

13. ABSTRACT *(Maximum 200 words)* This report describes the marked improvements made of the production line under the PVMaT program: successfully developed a high-speed, all-laser, monolithic integration process for CIGS-based modules on polyimide substrates; exceeded PVMaT goals for scribing rate and total interconnect width; developed robust, well-controlled techniques for selective scribing; improved CIGS evaporation sources to allow uniform, controllable delivery; completed foundation required to integrate higher CIGS deposition rates into the production line; developed well-controlled Se delivery system to minimize Se consumption; successfully integrated the parallel-detector spectroscope ellipsometer (PDSE) into a production CIGS deposition chamber; collected useful, in-situ data with PDSE; validated the performance of the X-ray fluorescometry (XRF) sensor in the production CIGS deposition chamber; and successfully incorporated the XRF sensor into the control architecture of the production CIGS deposition chamber.

14. SUBJECT TERMS: PV; laser scribing process; high-rate deposition; effusion source; real-time processing parallel detector spectroscopic ellipsometer (PDSE); X-ray fluorescometry (XRF); PVMaT; CIGS

15. NUMBER OF PAGES

16. PRICE CODE

17. SECURITY CLASSIFICATION OF REPORT	18. SECURITY CLASSIFICATION OF THIS PAGE	19. SECURITY CLASSIFICATION OF ABSTRACT	20. LIMITATION OF ABSTRACT
Unclassified	Unclassified	Unclassified	UL